EUROPEAN COMMISSION

nuclear science and technology

Oxide Fuels: Microstructure and Composition Variations (OMICO)

M. Verwerft[1], S.E. Lemehov[1], M. Wéber[1], L. Vermeeren[1], Ph. Gouat[1], V. Kuzminov[1], V. Sobolev[1], Y. Parthoens[1], B. Vos[1], S. Van den Berghe[1], H. Segura[2], P. Blanpain[2], J. Somers[3], G. Toury[3], J. McGinley[3], D. Staicu[3], A. Schubert[3], P. Van Uffelen[3], D. Haas[3]

([1]) SCK•CEN (BE), ([2]) AREVA NP (FR), ([3]) JRC-ITU (EU)

Contract N° FIKS-CT-2001-00141

Final report

Work performed as part of the European Atomic Energy Community's research and training programme in the field of nuclear energy 1998-2002 (Fifth Framework Programme)
Key action: Nuclear fission
Area: Operational safety of existing installations

Directorate-General for Research
2007 Euratom EUR 23104

Contents

List of abbreviations

EPMA	electron probe micro-analysis
LWR	light-water reactor
PWR	pressurised-water reactor
MCNP	Monte Carlo N-particle transport code
MOX	mixed oxide
SIMS	secondary ion mass spectrometry
FGR	fission gas release
SET	separate-effect test
IPS	in-pile section
MIMAS	micronised master blend
SOLMAS	sol-gel master blend
LAF	laser flash
DSC	differential scanning calorimetry
LVDT	linear variable differential transformer
SPND	self-powered neutron detector
LHGR	linear heat generation rate
OPS	out-of-pile section
PT	pressure transducer
TC	thermocouple
(ND) PIE	(non-destructive) post-irradiation examination
PCMI	pellet-clad mechanical interaction

Executive summary

In the project OMICO (Oxide Fuels: Microstructure and Composition Variations), the behaviour of three different fuel compositions (*UO_2, $(U,Pu)O_2$ and $(Th,Pu)O_2$*) has been studied. For each composition, two different microstructures were inter-compared (*homogeneous and fine dispersed ceramic-in-ceramic*). This resulted in six different fuel types which were assembled in a small experimental assembly and irradiated under representative pressurised-water reactor conditions. The primary objective was to provide insight in the *separate effects of fuel chemistry* (matrix composition) on the one hand *and the degree of dispersion of the fissile material* (microstructure) on the other hand.

The project OMICO incorporated several challenging objectives on nuclear fuels, requiring technological developments in various areas. The complexity of some of these technological developments was initially overlooked and/or their extent was underestimated, leading to substantially higher expenses at the research institutes JRC/ITU for manufacturing and SCK•CEN for irradiation than originally foreseen and a substantial delay of the project (66 months instead of the original estimate of 36 months). Despite its difficulties, OMICO did achieve important successes as well.

– The experimental OMICO assembly had to be calculated in a three-dimensional approach. At the time of start of the OMICO project, 3D Monte Carlo calculations were not yet established for the complex core of the BR2 reactor. The thorough cross-checks with the conventional 2D approach, comparison with reference programmes and the irradiation of a dummy assembly contributed to the confidence in the MCNP modelling of complex experiments in the BR2 reactor, and are today common practice.
– Fuel manufacturing to tight LWR specifications demonstrated once again ITU's key role as an independent experimental fuel manufacturer in Europe, and the OMICO programme has extended the core competence of this laboratory to heterogeneous $(Th,Pu)O_2$ and UO_2 fuels.

In terms of fuel-performance data, the OMICO experiment fully achieved the goals with respect to the acquisition of thermal data (power versus centreline temperature data-set). The unfortunate loss of the instrumented rods after five cycles didn't allow us to address the dynamic evolution of fission gas release through online measurements, but through two dedicated irradiation cycles on the non-instrumented rods, one of which contained a mild transient, did allow recovering in part the objective of fission gas release.

1 Objectives

The objectives as set forth in the project proposal and the modifications as introduced during its execution (updates of the description of work) are given below.

1.1 Scientific and technical context

To guarantee the *safe operation of nuclear reactors*, the behaviour of nuclear fuel under various operating needs to be assessed. For the *prediction of critical parameters* of fuel behaviour such as temperature profile, fission gas release (FGR) and cladding corrosion, *one relies upon code calculations*. These calculations make use of semi-empirical models that are fine-tuned for each fuel type. Calculated results are in general only accepted if the code itself has been validated for the specific fuel and operating conditions. Although such a validation procedure allows gaining confidence in the code predictions, *the evaluation* of the correctness and/or completeness *of the physical models needs* dedicated *parametric experiments*. This is essentially due to the fact that the measured features (gas pressure, fuel swelling, clad creep etc.) are functions of many parameters which are most often coupled non-linearly. Even though well-validated codes for MOX fuel currently exist, there is *still discussion on the role that is assumed by the specific microstructure of MOX*, especially regarding the release of fission gas.

The test matrix compares in a systematic way the behaviour of three different fuel compositions (*UO_2, $(U,Pu)O_2$ and $(Th,Pu)O_2$*). And for each composition, two different microstructures are inter-compared (*homogeneous and fine-dispersed ceramic-in-ceramic*). This results in six different fuel types which are assembled in a small experimental assembly and irradiated under representative pressurised-water reactor conditions (i.e. at 155 bar, 300 °C, with controlled water chemistry: 400 ppm B, $6.9 < pH_{300} < 7.4$ and 25 cc/kg $< [H_2] <$ 35 cc/kg). The primary objective is to provide insight into the *separate effects of fuel chemistry* (matrix composition) on the one hand *and the degree of dispersion of the fissile material* (microstructure) on the other hand.

Two sets of six fuel rods are produced, one set instrumented for pressure and temperature and a second set that can be unloaded at different intervals for non-destructive analyses. The online measurement of two essential parameters (gas pressure and central temperature), complemented by intermittent out-of-pile non-destructive tests, provides a set of data with which the calculated predictions of fuel behaviour are to be compared. The flexibility of irradiation conditions offered by a materials-testing reactor allows imposing specific irradiation conditions, the results of which are followed online to test various hypotheses on the response of the fuel. This wealth of information on the other hand has to be managed carefully by continuous efforts of interpretation and predictive calculations. It is through the combination of well-chosen irradiation conditions guided by code predictions that all experimental results can be fully exploited in terms of basic physical phenomena.

The post-irradiation analyses comprise in majority non-destructive investigation of axial power profile, burn-up increment, creep, oxide layer growth, and rod integrity. In view of the observed discrepancies between calculated and measured centreline temperature and to

recover the early loss of instrumented rods, some destructive analyses (puncture, optical microscopy and electron probe micro-analysis) are also included. More detailed destructive analyses, including further optical microscopy, detailed EPMA, radiochemical work, secondary ion mass spectrometry, etc. are carried out in the Sixth Framework Programme project LWR-DEPUTY.

1.2 Contribution to programme/key action objectives

The objectives of this proposal are in line with several objectives of the Fifth Euratom Framework Programme and in particular with the priorities set forward for proposals on nuclear fission submitted on 22 January 2001:

- In the topic 'evolutionary concepts' in Paragraph 2.2 of 'Operational safety of existing installations', it was specifically mentioned that actions on MOX fuel should focus on the *Development and experimental verification of improved best-estimate analytic tools (i.e. better models) in order to assess realistically the applied safety limits.* The OMICO project includes instrumented irradiation under realistic PWR conditions of a matrix of three different compositions, and for each composition two microstructures. This matrix allowed separate-effect testing (SET) of the influence of chemistry and microstructure on FGR. We expected obtaining better insight in fundamental aspects of the behaviour of mixed-oxide fuels regarding the release of fission gas. It was foreseen to validate existing and industrially applied codes with the experimental results and to propose an improved approach (model) to account for FGR in heterogeneous fuels. The combined effort of the institutes grouped together in the consortium would lead to a common understanding of MOX fuel performance in the European Union.

- There is a renewed interest in the use of thorium-based MOX fuels to minimise production of minor actinides (a topic which would fall under Paragraph 2.3 'Safety and efficiency of future systems'). Including thorium-based MOX in the present proposal is thus not only essential for the SET approach of the FGR problem, but also for the judgement about its use in future systems, for which it is essential that the in-pile behaviour can be realistically assessed. Although important experimental programmes on thorium-based fuels have been carried out in the past, none of the currently used fuel-performance codes include at present a mixed thorium-plutonium module. As thorium-based fuels will be part of the chosen matrix of experimental fuels, modules including the thorium material properties should be developed and/or improved, depending on the fuel-performance code.

The nuclear industry in Europe in general and MOX technology in particular have a leading position in the world. Only with continuous efforts to maintain and further develop the technology and knowledge, Europe can keep the highest standards of safety and efficiency on its nuclear market. The transfer of European expertise and technology is also only possible when these continuous efforts are maintained. To name just a few well-known domains of out-of-Europe interest, we can quote the Chinese market for nuclear technology, the Japanese market for MOX fuel in particular and the Russian-American interest in using LWR MOX for burning Pu-grade weapons.

2 Project work plan

The project work plan was divided in design (WP1), fuel manufacturing (WP2), detailed analysis of the unirradiated fuel (WP3), irradiation rig development, in-pile experiment (WP4), post-irrdiation examination (WP5), and theoretical developments (WP6). A graphical presentation of the relation between the individual work packages is given in the PERT chart below (Figure 1).

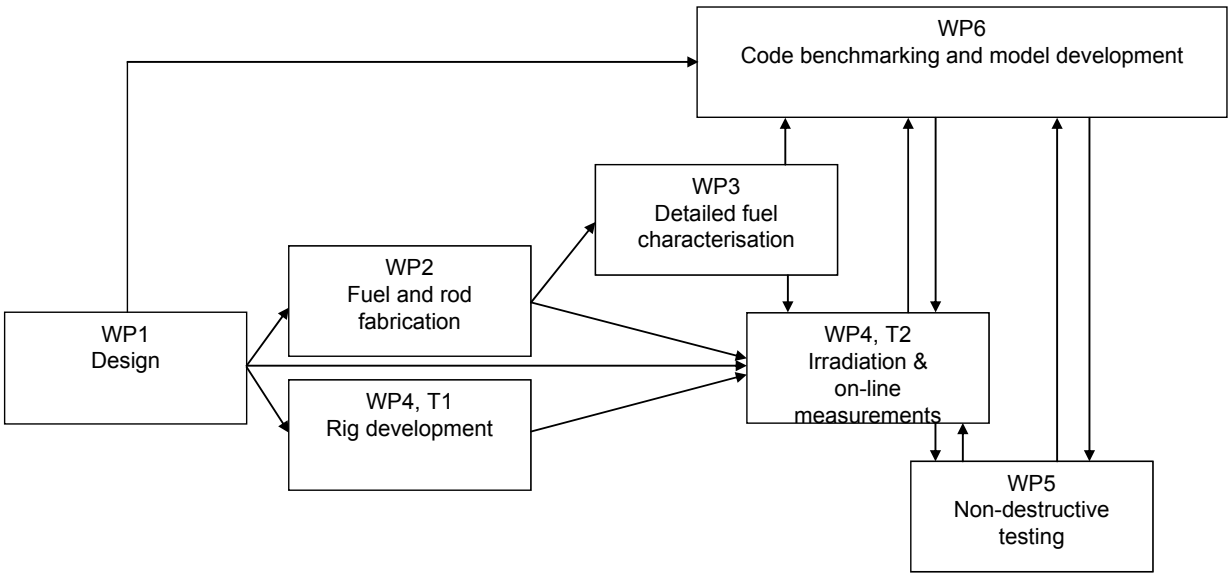

Figure 1: PERT chart of the OMICO project

3 Achievements per work package

The essential achievements obtained in the various work packages are given.

3.1 WP1 Design calculations

The research conducted in this work package resulted in five reports (Deliverables D1, D2a, D2b and D3 and one technical report). The design calculations consisted of iteration between the definition of requested power histories for all rods, the calculation of corresponding enrichments and irradiation conditions, and calculation of resulting thermo-mechanical evolution of the fuel rods.

The initial irradiation history [1] was determined on the basis of the OMICO targets: in order to study the thermal threshold for fission gas release, it was decided to aim at a few percent FGR during the second year of irradiation in the pressurised water loop CALLISTO of the BR2 reactor at Mol. Further constraints were imposed on the irradiation history: the threshold of fuel restructuring should not be reached, sufficient burn-up should be obtained within the given time frame (210 effective full power days), fissile isotope distribution should be representative etc. These constraints have led to a search for an optimal compromise between fuel pin diameter, fissile isotope content, irradiation conditions etc. The essential results of the design optimisation process are presented in Table 1.

Table 1: Design parameters of the fuel pellets [2]

		A	B	C	G	H	I
Fuel type		UO_2	$(Th,Pu)O_2$	UO_2	$(U,Pu)O_2$	$(Th,Pu)O_2$	$(U,Pu)O_2$
Technology		sol-gel	sol-gel	MIMAS	sol-gel	sol-mas	MIMAS
Enrichment *	wt%	9.0	8.0	9.0	9.1	12.8	9.0
Theoretical density fraction		0.96	0.96	0.95	0.96	0.95	0.95
Density	kg/m³	10522	9699	10412	10563	9658	10453
Grain size	µm	12	5	5	12	5	5
Maximum densification **	%TD	0.1	0	0.4	0.1	0	0.4
Pellet height	mm	7.14	7.14	7.14	7.14	7.14	7.14
Pellet diameter	mm	5.9	5.9	5.9	5.9	5.9	5.9

* Enrichment (x) was determined as a mass ratio:
$x = m_{U(235)}/m_U$ for UO_2 fuel;
$x = m_{PuO2}/m_{(Pu,U)O2}$ for $(Pu,U)O_2$ and (Pu,Th) MOX.
** Expected values.

The 3-D neutron transport code MCNP4C was used to assess the axial distribution of neutron flux and generated linear power. The detailed model of BR2 includes the nearly exact geometrical representation not only of the driver fuel elements with their axial burn-up distribution, but also of partially inserted control and regulating rods, of experimental devices

and of radioisotope production rigs which allows to take into account all perturbing effects. It is shown that the MCNP4C model of BR2, benchmarked with previous CALLISTO IPS1 experiments, gives satisfactory results.

The axial power profile of all rods is calculated in [3]. The values are normalised to a total power of BR2 of 57 MW. Due to this normalisation, the energy release per fission is averaged out over the reactor. Since most of the total power of the BR2 is due to fission in U^{235}, one may expect a slight underestimation of the linear power values in the MOX rods. (The average energy released by Pu^{239} fission being different from the average energy released by fission of U^{235}). Apart from the normalisation to the 57MW reactor power, no other correction factors were applied to the reported linear power. It is observed that in the present stage of calculations, end pellet peaking is insufficiently suppressed in all rods. The suppression of the end effects will be the subject of further optimisation of the Hf-Y oxide end pellet composition and dimensions. The MCNP calculations show that with the chosen configuration, irradiation conditions and enrichment, adequate power levels are obtained.

Evolution calculations are performed by solving the Bateman equations. From the initial enrichment of the OMICO pins (given in Table 1), and one-group microscopic cross sections weighted on the thermal spectrum reached in the CALLISTO IPS1 device, the Bateman equations are solved. During the five first cycles, corresponding to $5 \times 21 = 105$ days of irradiation at full power, the total BR2 power is 57 MW and the two adjacent channels (channel F46 and G60) are loaded with driver fuel elements with a burn-up of 48 %. After the first five cycles, one of the two adjacent channels (channel F46) is loaded with a fuel element with a burn-up of 20%, while the total BR2 power is maintained at 57 MW. Of course the flux level and the set of one-group cross sections are updated for the evolution of the isotopes during the following five cycles of BR2. After ten cycles, the two adjacent channels are loaded with two fuel elements with a burn-up of 20% and the total power of BR2 is increased by a factor of 1.08. The results of the evolution calculations show that the objectives of LHR and burn-up can be maintained throughout the duration of the project (i.e. 10 BR2 cycles of 21 days each) and that sufficient margins on the operating conditions are available at the end of the second year of irradiation for power adjustments or even for prolongation of the irradiation.

In the preliminary design calculations, several simplifications were adopted for the evolution calculations. The neutronic calculations were performed in a 2D approximation (DORT-code) and the neutron flux was assumed to be constant in time during five cycles. These simplifications only hold to a certain extent. In fact, the flux depends on the burn-up of the pins and the BR2 driver fuel elements, and is not constant. More accurate calculations need iterations between transport and evolution code calculations and fall outside the scope of preliminary design calculations but will be performed when the fabrication is finished. It should also be stressed that the effect of the presence of fission products is presently not taken into account in the evolution calculations. It is also known that the build-up of fissile U^{233} is not correctly accounted for, which partly explains the rapid power decrease for $(Th,Pu)O_2$.

The thermo-mechanical design calculations were performed with the light-water reactor fuel-performance code FEMAXI-V. The code version that is used includes the material properties for UO_2 as well as $(U,Pu)O_2$ and allows to perform design calculations for either fuel up to intermediate to high burn-up. It should be stressed, however, that while the code version allows performing MOX calculations, it explicitly states that a detailed assessment is not

recommended for MOX. There are no material properties included in the standard version of the code for $(Th,Pu)O_2$ MOX evaluation, and the preliminary material properties inferred from data in the open literature were integrated in a separate version of the code, compiled for the purpose of performing design calculations for the OMICO project. The main results for are given in Tables 1 and 2.

After the first iteration between neutronic and thermo-mechanic calculations with the FEMAXI code, the thermo-mechanic codes TRANSURANUS (ITU) [4] and COPERNIC (AREVA NP) [5] were also involved in the design process. The calculation of the three codes all confirmed that the project targets as well as the safety criteria in terms of melting temperature and inner pressure are well respected in all fuel segments.

During the preparation of the OMICO programme, a detailed assessment of the results obtained in the course of the running experiment BACCHANAL was performed. The latter experiment is loaded in the same in-pile section (IPS 1) that is selected for the OMICO experiment. The immediate cause for such an assessment relates to the problems with power predictions. Indeed, in the course of refining the neutronic calculations for the OMICO rodlets, it became apparent that 3D effects are not negligible. Earlier calculations were performed using a 2D code (DORT) that could be calibrated to the running experiments, although it was known that the absolute values for fission power predicted for experiments in the considered IPS1 of CALLISTO exhibited a systematic deviation. Since the BACCHANAL experiment could rely upon past experimental results for absolute power calibration, the deviations of the code predictions were accepted. This is no longer the case for the OMICO experiment, where important 3D effects were detected using MCNP calculations.

Parallel to the calculation of the OMICO experiment, full core calculations were performed for the reference irradiation cycle (cycle 5 of 1998) of the BACCHANAL experiment. For the given irradiation cycle, in-pile measurements and gamma spectrometry results are available. From the assessment of the latter experiment, it could be deduced that the MCNP predictions seem to underestimate the true power by about fifteen percent. Since there is insufficient experimental evidence for adopting a *brute force* method of adjusting the predicted power by this value, the fifteen percent difference is currently regarded as the error margin for the calculations. This has been the subject of discussion with the management of the BR2 reactor, since the margins between the true power and predicted power should be met by additional flexibility of the BR2 reactor. It was concluded that the error margins are sufficiently small to call upon the flexibility of BR2 operation for adjustment. It has to be noted that during the execution of the project, the true power will be assessed by several independent methods (CALLISTO loop instrumentation, fuel rod instrumentation and out-of pile intermittent gamma spectrometry).

3.2 WP2 Fuel and pin fabrication

3.2.1 Fuel fabrication

Work Package 2 covers the fabrication, assembly in rods and transport of six different fuels: three different fuel compositions (UO_2, $(U,Pu)O_2$ and $(Th,Pu)O_2$), and for each type, two different microstructures are compared (homogeneous and heterogeneous). For each fuel, two pins are produced: one instrumented and one non-instrumented, yielding thus in total twelve

fuel pins. The three homogeneous fuels (A, B, and G) were produced by the sol gel process, while the heterogeneous fuels were produced by the MIMAS (C and I) and SOLMAS processes (H). The results are reported in the fabrication report (Deliverable D5, [6]).

In the sol gel process (fuels A, B and G), the constituent elements are dissolved in aqueous solution and, following analysis, are mixed in the appropriate amounts. The desired quantity is mixed with polymers to increase the viscosity and is then dispersed using a rotating cup atomiser. The resulting droplets are collected in an ammonia bath, where a droplet to particle conversion occurs via a gelation process. Following ageing, the beads are washed in water and calcined before being compacted into pellets, which are then sintered at a suitable temperature and in an appropriate atmosphere to give the product pellets.

The SOLMAS process is used to fabricate the heterogeneously dispersed (Th, Pu)O_2 fuel for pin H. The sol gel process is used as described above in to produce particles of (Th,Pu)O_2, which are then blended with ThO_2 powder, before being pelletised and sintered. The Pu/(Th + Pu) content in the beads is significantly higher than in the final pellet. Thus the final Pu content is selected by variation of the dilution ratio. The (Th,Pu)O_2 particles are near spherical from the sol gel process and are not sieved. The particle sizes are in the 20-120 μm range.

The MIMAS (micronised master blend) process is based solely on powder metallurgical methods and is used to produce two fuel pins (C and I). In this process a high enriched "primary blend" (also called master blend) is produced by a powder milling step. The resulting powders are sieved forcibly through a sieve with selected dimensions. The secondary blend with the required enrichment is formed by mixing the primary blend with UO_2 powder, which can also be sieved. Following the addition of lubricants, the secondary blend powder is compacted into pellets, which are sintered under a suitable atmosphere to obtain final product pellets with specified density, O/M, grain size in the UO_2 phase, and particle size of the primary blend. The primary and secondary blends should be sieved preferably at 40 μm to give the best possible distribution of the high enriched particles throughout the pellet. For MOX fuels, the primary blend is 30 % enriched in plutonium (Pu/(U + Pu)), while for the heterogeneous UO_2 fuel, the primary blend is obtained by co-milling high enriched (80 % ^{235}U) and depleted UO_2.

In general the pellets had a good visual aspect. All specifications concerning the chemical composition (enrichment of the fissile component in the master blends and final pellets and O/M) were met in full. The fabrication data are presented in full in Deliverable 5. Some essential dimensions and other characteristics of the pellets are given in the tables below.

Table 2: Pellet characteristics

Batch	Fuel type	Enrichment		Diameter	Density	Thermal stability
		$^{235}U/\Sigma HM$	Pu/ΣHM	(mm)	(% TD)	(Δρ)
A	UO_2	8.933	-	5,907	96,0	-3.73%
B	$(Th,Pu)O_2$	-	7.923	5,905	98,0	-0.35%
C	UO_2	9.195	-	5,901	95,2	1.17%
G	$(U,Pu)O_2$	-	9.06	5,904	96,1	-0.26%
H	$(Th,Pu)O_2$	-	12.814	5,903	96,6	-0.77%
I	$(U,Pu)O_2$	-	9.03	5,903	95.7	-0.17%

Deviations between specifications and final as fabricated density of the two thoria-based fuels do occur but were accepted on the argument that at the time of fabrication, the status of the project prohibited the repetition of these fabrications as this would have caused important additional delays. As the pellets densify slightly during the initial period of the irradiation, an out of pile thermal stability test (1700 °C for 24 hours under an Ar atmosphere) was performed and the pellets show an acceptable behaviour.

The $(U, Pu)O_2$ and $(Th, Pu)O_2$ fuels were fabricated with high fissile content plutonium (see Table 3). The heterogeneous fuels (MIMAS process for fuels C and I and SOLMAS process for fuel H) employ a primary blend of 30 % enrichment (see Table 4).

Table 3: Pu isotopic vector (reference date of analysis: 12.11.2002)

	Weight percentage
Pu 238:	0.012
Pu 239:	91.500
Pu 240:	8.304
Pu 241	0.140
Pu 242:	0.044
Am 241:	0.685 (relative to Pu)

Table 4: Primary blend composition of the heterogeneous fuels

Fuel		Process	Enrichment (wt%)	
C	$(U,U)O_2$	MIMAS	$^{235}U/Utot$	29.42%
I	$(U,Pu)O_2$	MIMAS	Pu/(U+Pu)	29.57%
H	$(Th,Pu)O_2$	SOLMAS	Pu/(Th+Pu)	29.72%

Ceramographic examination of the pellets showed that no defects were present. Results exhibiting the grain size in the fissile component are shown in Figure 2 below. The grain sizes are consistent with the specified values. For the UO_2 fuels (A and C), the grains are very uniform, and those of the sol gel material (A) are larger than in the pellets produced by powder metallurgy (C). Etched samples of the $(U,Pu)O_2$ fuels show a very uniform grain

distribution in the homogeneous fuel (G) and the heterogeneous nature of the MIMAS Fuel I. A similar observation is made for the (Th,Pu)O_2 fuels. The grains in the homogeneous fuel (B) are uniform. In contrast, the Pu etching of Fuel H shows much greater heterogeneity.

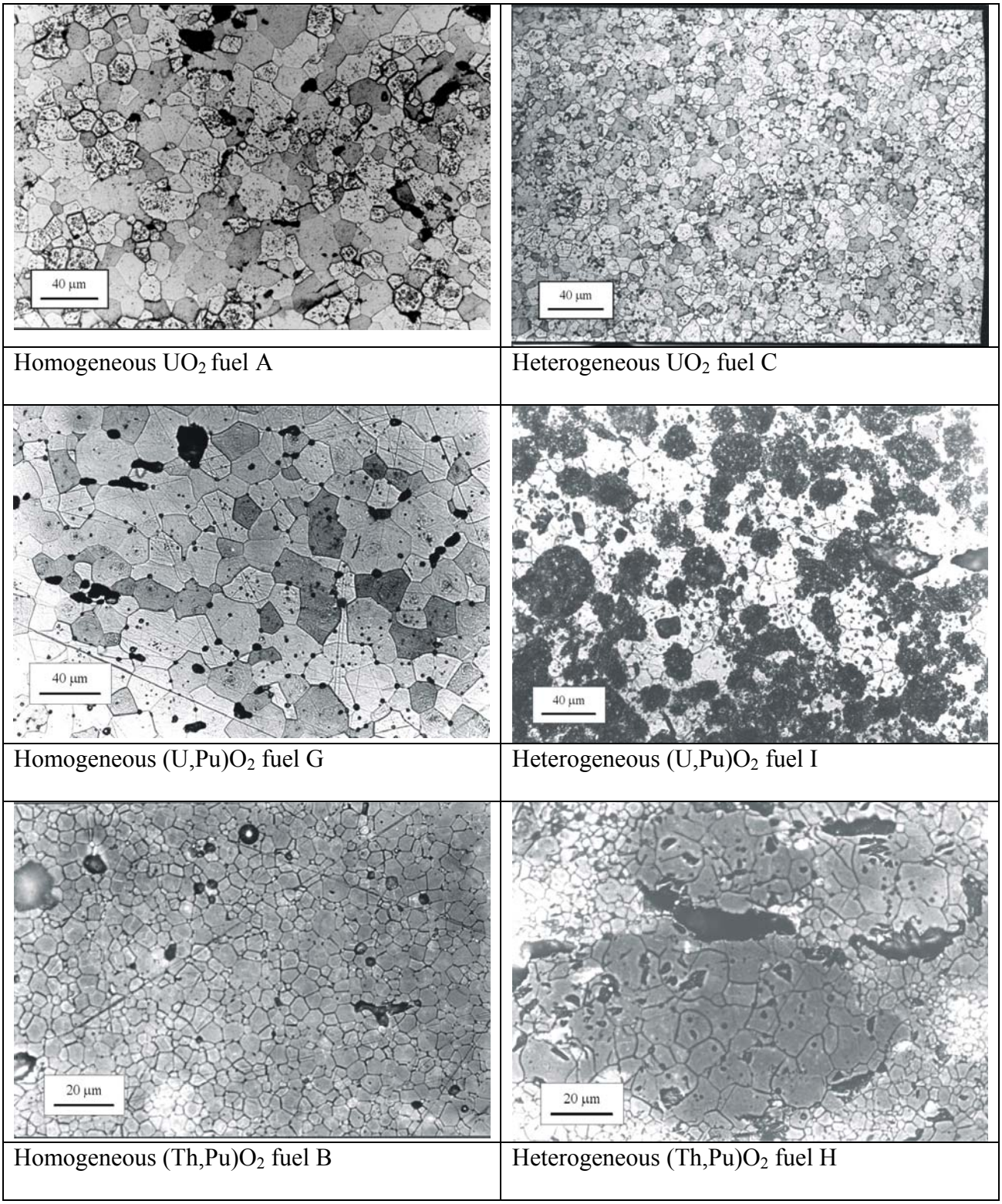

Homogeneous UO_2 fuel A	Heterogeneous UO_2 fuel C
Homogeneous (U,Pu)O_2 fuel G	Heterogeneous (U,Pu)O_2 fuel I
Homogeneous (Th,Pu)O_2 fuel B	Heterogeneous (Th,Pu)O_2 fuel H

Figure 2: Overview of the ceramographs (grain-etched state) of the different fuels produced in OMICO

3.2.2 Pin welding

The fabrication of the fuel pins requires a series of pre-tests to determine the correct parameters. This is then qualified by performing a series of tests at the optimal conditions and off optimal conditions. The latter are set to deepen the weld (1 Amp extra and the electrode set 0.1 mm closer) and less deep (1 Amp less and 0.1 mm further away). This gives the conditions Opt+ and Opt-. Pairs of welds are made at each of these conditions and then they are sectioned axially and radially through the weld before being polished and etched to reveal the weld depth. An example for the non-instrumented fuel pins lower cap is shown in Figure 3 below.

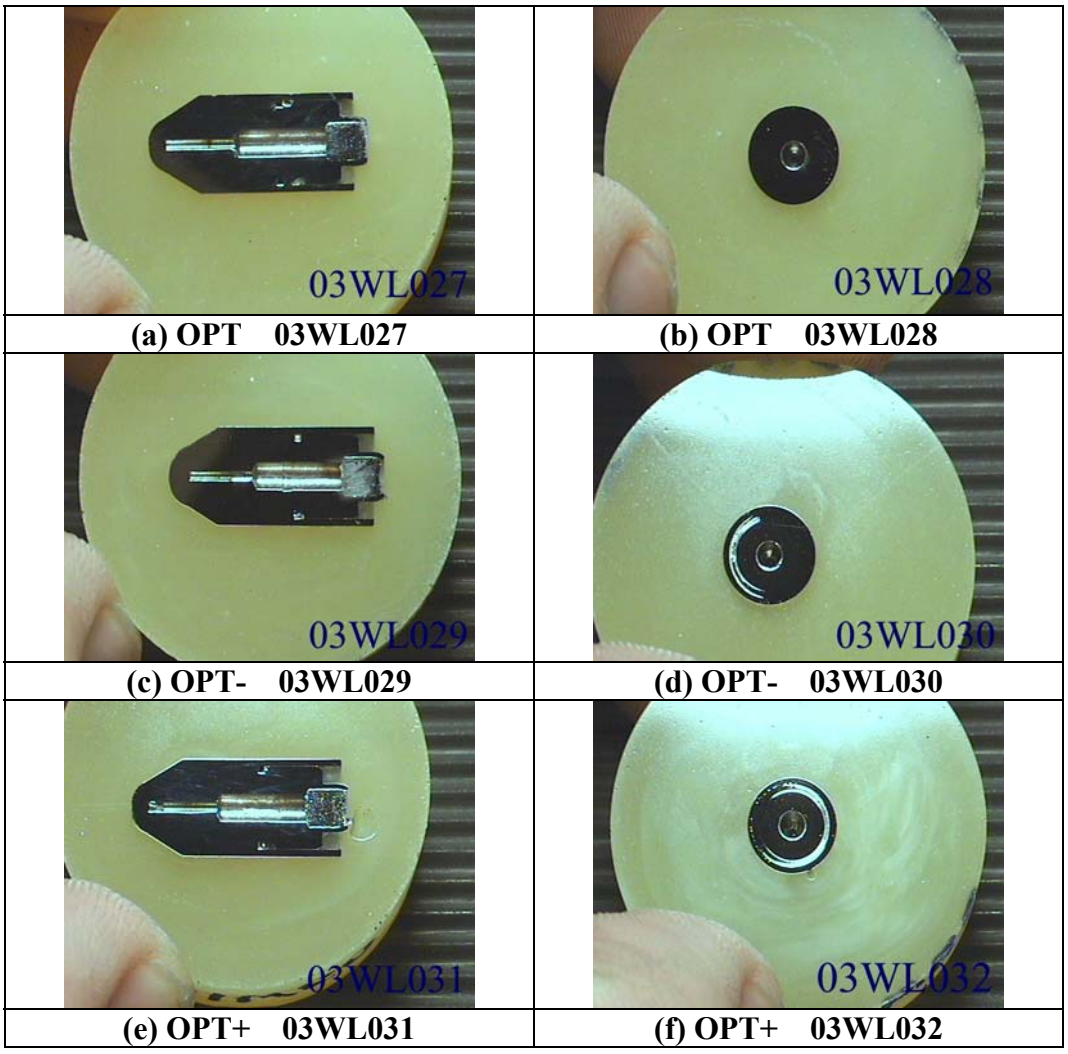

Figure 3: Examples of the qualification welds for pin welding. Optimal conditions (a and b) and off-optimal conditions (c to f)

Welding of the instrumented fuel pins was an extremely complex procedure and caused substantial additional delays on the whole project (11 months) which was totally unforeseen. The main cause for this delay was an insufficient corrosion resistance of the welds due to atmosphere contamination. The final implementation of Ar atmosphere in the welding glove boxes proved to be successful: in the last quarter of 2003, the non-instrumented pins were welded and in the second quarter of 2004, the instrumented pins were welded successfully.

Final controls on the welded pins (visual, dimensional, X-ray, He leak test at room temperature and at 300°C, surface contamination level and dose rate) were accepted.

Transport of the fuel pins took place on 30-06-2004 (departure from ITU) and 1-7-2004 (arrival and unloading at SCK•CEN).

3.3 WP3 detailed fuel characterisation

Detailed fuel characterisation comprises essentially ceramographic observations and their analysis and the thermal diffusivity and heat capacity measurements. These analyses are reported in Deliverable 6 [7].

3.3.1 Ceramographic observations

The porosity distribution in Fuels A and C differs remarkably. While Fuel C shows a relatively even porosity distribution of relatively small size, Fuel A shows somewhat larger pores, but also extensive regions of high density with no large pores. There appears to be only small pores (of less than a few μm) in these regions. The latter is an artefact of the sol gel production route and has been observed in other campaigns. It arises due to the very high sinter activity of this type of material and causes several precursor particles to sinter together in an extremely effective way. Also lenticular pores are formed occasionally as there is a memory of the original particles and in extreme cases, their location can be identified by semi circular pores or even partial rings of small pores.

The porosity distribution in Fuels B and H also differ markedly. Fuel B shows a relatively homogeneous porosity distribution. The majority of the pores are near spherical and there is some evidence that they are located in arcs, presumably following the location of the precursor spherical particles. Some lenticular pores are also observed. The polished surfaces of Fuel H also show semicircular pores. This indicates the boundary between the 30% Pu enriched beads and the ThO_2 matrix.

Also for fuels G and I, the porosity distribution differs. While Fuel I shows a relatively even porosity distribution probably in two size regimes, Fuel G exhibits extensive regions of high density with only small (less than a few μm) pores. As described above for Fuel A, the latter is an artefact of the sol gel production route. Lenticular and near-spherical pores are observed also.

The porosity distribution has been measured from the polished ceramographs using image analysis. This was made at a single position midway between the centre and the periphery on radial sections. The results are given in Table 5.

Grain size is reported in Table 6.

Table 5: Porosity distributions

Fuel	A	B	C	G	H	I
0-1 µm	558 (70.81)	323 (69.02)	996 (48,87)	366 (57.55)	197 (32,83)	409 (32,33)
1-2 µm	149 (18.91)	67 (14.32)	889 (43,62)	172 (27.04)	282 (47,00)	709 (56,05)
2-4 µm	43 (5.46)	50 (10.68)	150 (7,36)	68 (10.69)	99 (16,50)	127 (10,04)
4-10 µm	35 (4.44)	24 (5.13)	3 (0,15)	23 (3.62)	19 (3,17)	16 (1,26)
10-20 µm	3 (0.38)	4 (0.85)	0 (0,00)	7 (1.10)	3 (0,50)	4 (0,32)
Total count	788	468	2038	636	600	1265
% area	3	2	4	4	4	5

Table 6: Grain size (MLI) of the OMICO fuels

Batch	Fuel	Fissile component	Matrix component
A	UO_2	17	
B	$(Th,Pu)O_2$	4	
C	$(U,U)O_2$	6	6
G	$(U,Pu)O_2$	18	
H	$(Th,Pu)O_2$	11	ca 3
I	$(U,Pu)O_2$	10	≈ 3 *

* Very difficult to determine.

3.3.2 Thermal conductivity analysis

Thermal conductivity is derived from measured thermal diffusivity, specific heat and density. In this summary report, only the method and final results are reproduced.

The thermal diffusivity has been measured using a laser flash (LAF) method. The thermal diffusivity has been measured on the homogeneous $(Th_{0.91}Pu_{0.09})O_2$ fuel (OMICO B) as well as samples pressed from the master blend for the heterogeneous fuel, i.e. $(Th_{0.71}Pu_{0.29})O_2$. In addition the thermal diffusivity has been measured on the homogeneous U-MOX fuel (OMICO G).

In all cases the thermal diffusivity is lower, in the ascending set of conductivity as a function of temperature. In the descending measurements, the sample has already seen a high temperature and influence of self irradiation damage due to α emitters is removed. Therefore the reference result is always that of the descending measurement. The results themselves are potentially interesting as they reflect recovery ability of the fuel, but this is not the subject of these studies. It is noteworthy that the effect is highest in the sample with highest Pu content.

The thermal diffusivity of the Th MOX fuels is about 50% higher than for the U-MOX fuels at the lowest temperatures, but is almost a factor of 2 higher at 1500 K.

Differential scanning calorimetry (DSC) was used in this study to measure the specific heat. DSC measurements on all the samples were carried out in the temperature range 400-1450 K by applying a heating rate of 20 K/min with a purging argon gas flow rate of 100 ml/min. A disk of sapphire was used as a specific heat standard. The accuracy of the measurements is about 5 %.

The thermal conductivity λ (T) (in W $m^{-1}K^{-1}$) was calculated from the thermal diffusivity, α(T) (in m^2 s^{-1}), the heat capacity, C_p(T) (in J kg^{-1} K^{-1}), and the density ρ(T) (in kg m^{-3}). Thermal diffusivity changes due to variation of the sintered porosity were normalized to 5% porosity by using the relation:

$$\lambda_{95}(T) = \frac{1 - 0.05\, f(T)}{1 - P\, f(T)} \alpha(T)\rho(T)C_p(T)$$

where f(T) = 2.6-0.5 T/1000 and P is the porosity fractional volume.

The thermal conductivity values corrected for 95% density of the samples are plotted in Figure 4. For comparison, literature curves for UO_2 [8], (U,Pu)O_2 MOX with low (3 to 15 %) Pu content [9] and ThO_2 [10] are also shown.

The thermal conductivity of Pin G (U-MOX) is in very good agreement with that published by Duriez. The thermal conductivity of pin B (Th- MOX) is slightly lower than that for pure ThO_2 given by Pillai. At low Pu content, the thorium dioxide based fuel Pin B has a higher thermal conductivity compared to uranium dioxide, or (U,Pu)O_2.

The thermal conductivity of U-MOX fuel is lower than UO_2 as addition of small amounts of PuO_2 in the fuel decreases the thermal conductivity. Variation of the Pu content between 3 and 15 % does not appear to further decrease the thermal conductivity. If, however, the amount of Pu is increased above 15% then there is an additional decrease of the thermal conductivity of MOX fuel [9]. The correlation of Inoue [11] for FBR high Pu content U-MOX is also plotted for comparison, O/M = 1.99 was chosen.

A similar effect of the addition of Pu is observed here for the Th-MOX fuel. A moderate decrease in thermal conductivity is observed for 7.9% Pu. For 30 % Pu content, the decrease in thermal conductivity is stronger.

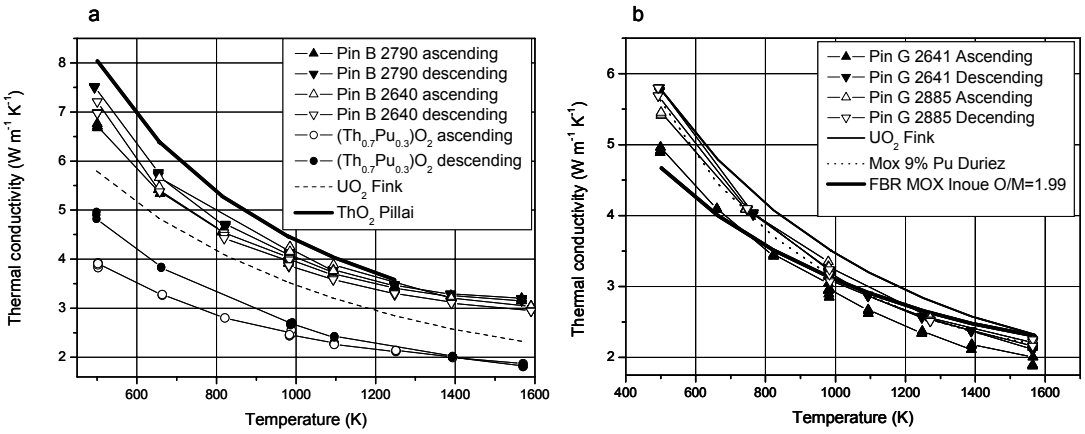

Figure 4: Thermal conductivity values. For comparison, literature values are also given.

3.4 WP4 Rig construction (T1) and irradiation experiment (T2)

3.4.1 Task T1 Rig construction

The rig consists of two main parts: the in-pile section (IPS), which includes all the components directly connected to or coming in the reactor vessel, and the out-of-pile section (OPS), which is made of the instrumentation rack, of the control panel, of the data acquisition system and of the "software packages" (i.e. the online power measurement, the FGR pressure and central line rod temperature measurement analysis). Rig modifications are reported in Deliverable 7 [12].

3.4.1.1 In-pile section (IPS) construction

The in-pile section (IPS) is similar to a standard CALLISTO IPS, but two modifications are introduced at the core level and at the head. Due to the electrical cables, the basket (shroud tube) containing the instrumented fuel rods cannot be separated from the suspension tube in the pool. Therefore, the shroud tube is split into two parts: the upper part with the instrumented rods will be fixed to the suspension tube and it will remain so attached to the end of the experimentation, while the lower basket can be disconnected by means of a special bayonet coupling. To avoid unexpected decoupling during IPS loading operation, a two steps movement has to be done, requiring a special tool. After uncoupling in the pool, the lower basket should then be transferred to the hot cell for non destructive testing and finally, it will be reassembled to the upper basket and loaded back into the IPS.

In order to keep the thermal flux at the fuel rods position as high as possible, the shroud tube should have almost the same wall thickness everywhere and its material should be Zircaloy-4. It has a cylindrical tube instead of the standard square tube because the bayonet coupling between the two parts requires a cylindrical shape. The tube dimensions and the pitch between the rods have been thermo-hydraulically optimised. The mechanical transition from Zircaloy-4 to stainless steel (bolting solution) is just above the core level. The fission gas pressure transducer, i.e. a bellow coupled to a LVDT, has a 13 mm diameter, therefore it is geometrically impossible to put eight of them on the same IPS level because the IPS inside

diameter is only 43 mm. To allow for equipping the eight fuel rods, the transducers are fixed on two separate levels in the stainless steel suspension tube, where 2 thermocouples are fixed to allow for temperature compensation in the pressure gauges, which are connected to the rod with a Zircalloy-4 capillary tube. This solution leads also to protect these detectors from the neutron and from very high gamma fluxes. The upper part of the IPS has been modified to reduce free convection, leading so to smaller axial heat losses (see also § 3.4.2.2).

The OMICO irradiation experiment requires extensive instrumentation, not only of the fuel rods themselves (pressure and temperature), but also neutron measurement (to allow online assessment of the irradiation conditions) and coolant temperature measurements (for general operating of CALLISTO as well as for thermal balance: bundle power registration). The CALLISTO In-Pile Section upper flange was extensively modified to allow the feed through of approximately 40 instrument read-out cables. It has been qualified according to the ASME III Class 1 construction code.

3.4.1.2 Out-of-pile section (OPS) construction

The out-of-pile section construction consists of the instrumentation rack and the data acquisition system. The instrumentation rack provides three main functions:

- The electronic unit for reading out LVDTs is the larger part of the instrumentation rack: it is made of 8 independent systems, which have a 400 Hz – 50 mA power supply to feed the primary coils and a high accuracy voltmeter to measure the output signal from the secondary coil.
- The alarm unit: as a back-up of the gas leak control system, the humidity is also detected inside the IPS instrumentation head by measuring the electric conductivity. When this conductivity reaches the fixed level, an alarm signal is actuated and transmitted to the reactor control room.
- All the thermocouples used to measure accurately the temperature differences are connected to the isothermal box, together with the reference temperature sensor (TE20). To reach reliable thermal balances in the OMICO experimental device, very precise measurements are required because the absolute temperature differences are rather small (< 10°C).

The data acquisition system of OMICO (an Agilent data logger connected to a PC) is developed as a sub-system incorporated in the general BR2 data acquisition system (BIDASSE server). Its first task is to get and store the raw signals from the detectors dedicated to the OMICO experiment (FGR pressure detectors, thermocouples, SPNDs and humidity detector). All the 60 channels are scanned every 1 or 2 minutes. This rack is located on the 4th floor in the BR2 control building, near the instrumentation rack. Second, another PC is connected to the BIDASSE server and calculates the online linear power of the separate fuel rods. It also processes signals from detectors and converts them into engineering unit.

A back-up data logger, on which vital channels are connected, is used to perform manually the determination of the rod power allowing to continue operating the reactor in case of BIDASSE-OMICO failure.

3.4.2 Task T2 Irradiation experiment

3.4.2.1 Irradiation history

The OMICO experiment was loaded during seven cycles in IPS1 of the pressurised water loop, CALLISTO. The power history is reported in Deliverable 8 [13, 14], and the monitoring of various thermo-hydraulic, chemical parameters is given in Deliverable 9 [15]. Due to rod failure, rod C (heterogeneous UO_2) had to be unloaded after four irradiation cycles. The rod was replaced by a dummy zircaloy bar of the same dimensions and the OMICO experiment was reloaded the subsequent cycle. A second failure of an instrumented rod led to the decision to unload all other instrumented rods and to continue the irradiation for two cycles more with the non-instrumented rods only.

In Figure 5, the overview of the reactor operation (BR2 total power) and the average power of one of the non-instrumented rods are given. It is obvious from this figure that the reactor power is only partly correlated with the power of an individual rod. While the OMICO experiment remains in the same position in the reactor, the rearrangement of the BR2 driver fuel elements allows one to increase or decrease the neutron flux locally (Figure 6). For cycle 2004/5, one driver fuel element was loaded in a channel adjacent to the OMICO experiment (F46), for cycles 2005/1, 2005/2, 2005/3, 2005/4 and 2006/3, no driver fuel elements were loaded in the channels adjacent to IPS1. During the last cycle (2006/4), driver fuel elements were inserted in two channels adjacent to OMICO (G60 and F46).

The reactor loading scheme defines the nominal power of each cycle (100%), which generally corresponds to ~ $60MW_{th}$. For specific purposes, the reactor can be operated at regimes different from the nominal power. Non-nominal operation conditions of course have their impact on all other experiments. During cycle 2004/5, OMICO limited the reactor operation to 82% of its nominal power (57 MWth) for several days and to 92% for the majority of the cycle. A detailed description of the first cycle operation is given in Deliverable 8a [13], and the description of all cycles in Deliverable 8b [14]. During cycle 2006/4, the OMICO experiment required a reactor power of 115% during 48 hours in order to obtain the FGR threshold power.

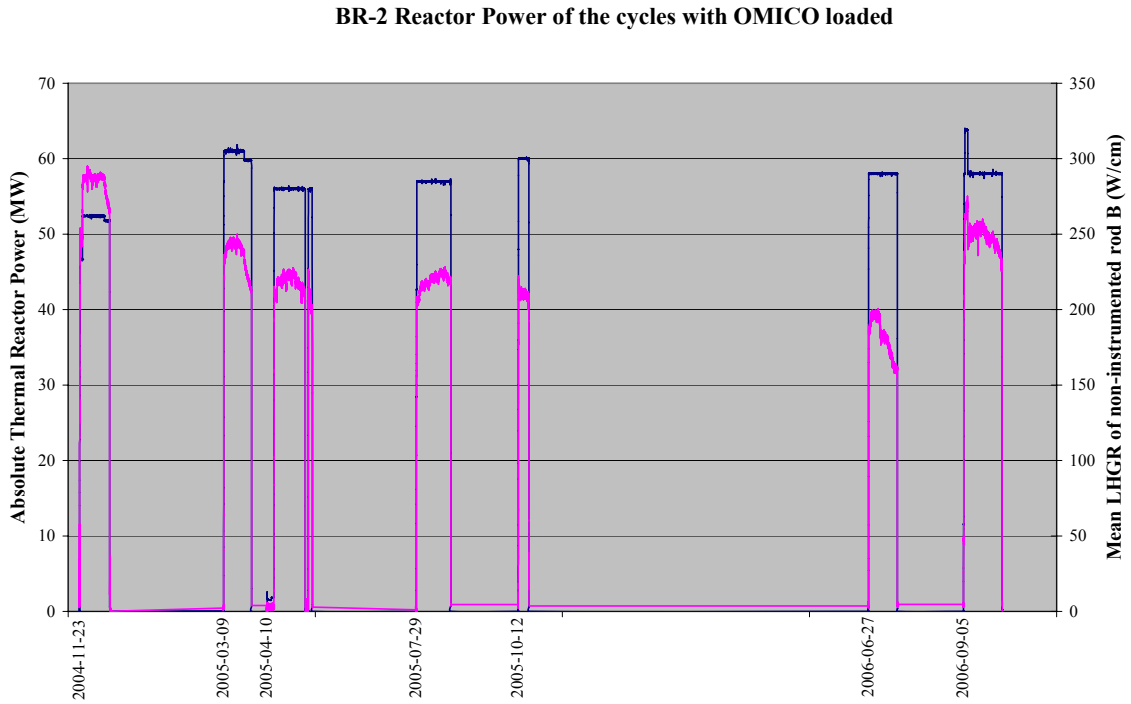

Figure 5: Reactor power (left axis, MW_{th}) and LHGR of non-instrumented rod B (right axis, W/cm). Note the variation within each cycle for the LHGR of an individual rod due to control rod movement

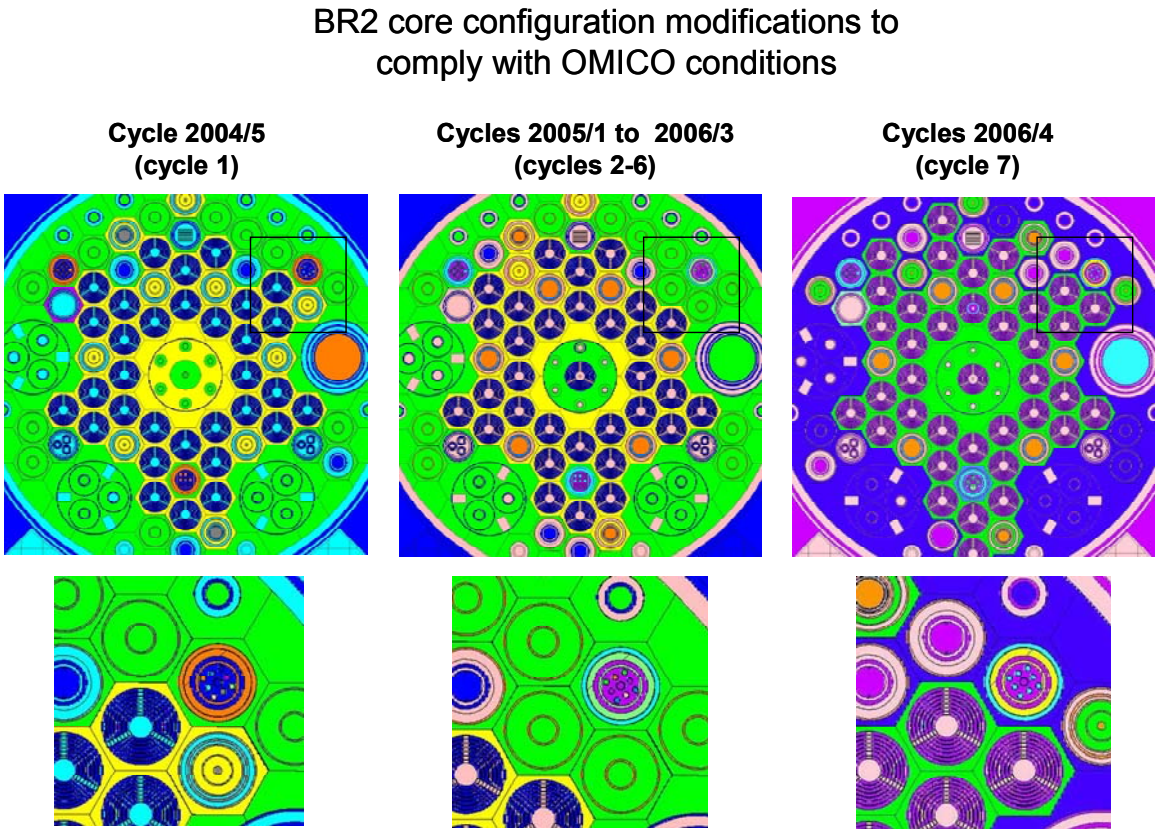

Figure 6: In the course of the experiment, the BR2 core configuration was modified in the region close to the OMICO experiment in order to obtain the requested linear power. Cycle 1: one driver fuel element in front of the OMICO position, cycles 2 to 6, no fuel elements in the channels in front of OMICO and for cycle 7 (FGR cycle): two fuel elements loaded in front of OMICO

3.4.2.2 Online power recording

The online power determination for the OMICO project is based on the thermal balance methodology, used successfully in many BR2 irradiation experiments [16]. It makes use of the instantaneous mass flow rate, corrected for the different losses, and measured temperatures at inlet, outlet and intermediate levels of the irradiation rig. The highest reliability could be obtained by using the thermocouples reading the temperature at inlet and outlet of in-pile section 1 (IPS1) of the high pressure loop (CALLISTO) in which OMICO is loaded (T_{in} and T_{out} in the schematic drawing of Figure 7). The measured enthalpy increase ($Q_{measured}$) is expressed as follows:

$$Q_{measured} = G_{CALLISTO} \times \left[H\ (T_{outlet}, P_{outlet}) - H\ (T_{inlet}, P_{inlet}) \right] \qquad (1)$$

where

T_{inlet} (T_{outlet}) is the water temperature at the inlet (outlet) of CALLISTO-IPS1
P_{inlet} (P_{outlet}) is the water pressure at the inlet (outlet) of CALLISTO-IPS1
$H(T,P)$ is the water enthalpy calculated as a function of temperature and pressure
$G_{CALLISTO}$ is the mass flow rate of CALLISTO-IPS1.

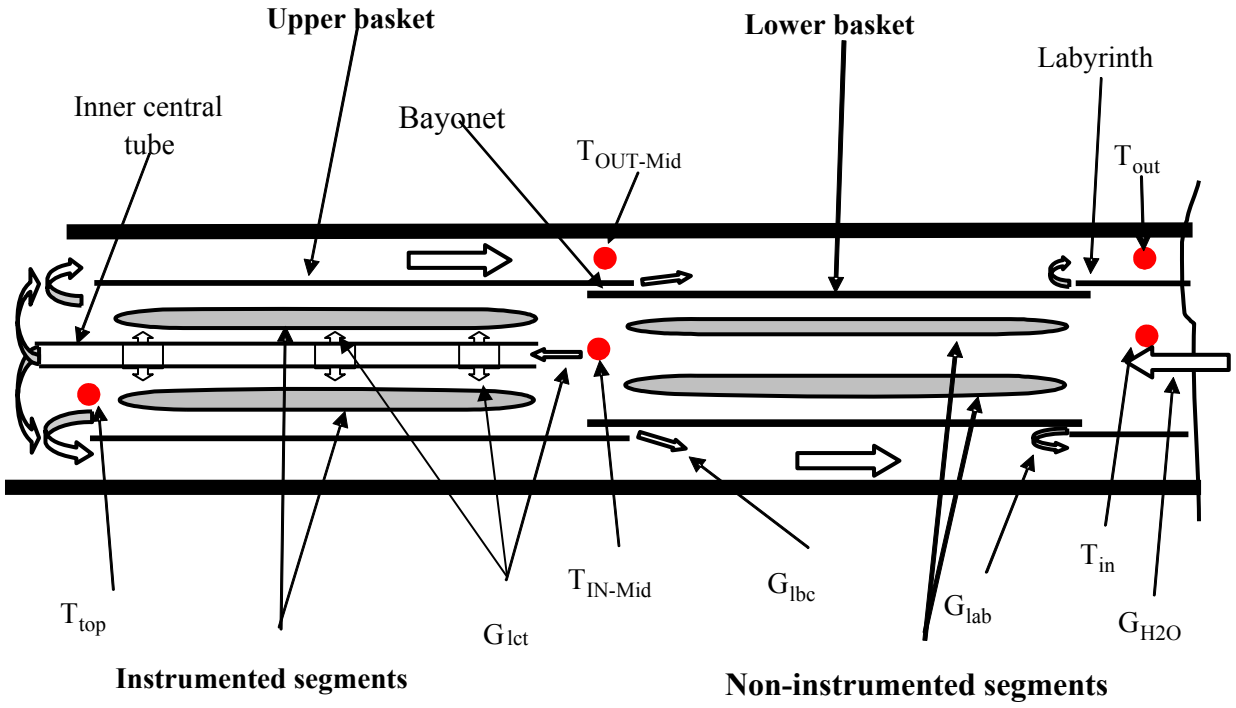

Figure 7: Schematic drawing of the thermal balance as it is implemented in the OMICO experiment. The different levels of thermocouple readings are indicated ("T"), as well as the mass flows, flow reversal point and various mass flow losses ("G")

The measured value must be corrected for radial and axial heat losses. The total power delivered to the coolant by the OMICO device (i.e. fuel rods and structural materials) is thus expressed as:

$$Q_{tot} = Q_{measured} + Q_{loss,radial} + Q_{loss,axial} \qquad (2)$$

The radial heat losses from the CALLISTO pressure tube to the BR2 water can be modelled analytically since the essential parts have a cylindrically symmetric configuration. Radial heat losses through the CALLISTO pressure tube amount up to 39kW/m^2.

The axial heat losses are more difficult to model since they are highly dependent on the exact geometry. When CALLISTO operates at PWR conditions (300°C), the water in the section above the flow reversal point of OMICO will come to a regime of free convection. In this regime, the axial heat losses are of the same order as the radial heat losses. The axial heat loss amounts to approximately 15kW when CALLISTO is operated at 300°C and must be calibrated prior to each cycle in the hot stand-by condition (reactor power 0MW, during heating up of CALLISTO to 300°C).

3.4.2.3 Power distribution in the OMICO rig (MCNP calculations)

The online thermal balance measurements determine a single value for the total energy (Q_{tot}) deposited in the cooling water of OMICO (corrected appropriately for losses). The

distribution of this power over the different sources is done on the basis of neutronic calculations.

Before each cycle, MCNP calculations are performed for the actual BR2 core configuration (such as given in Figure 8) and OMICO fuel composition. Since the cycle configuration may be subject to minor modifications up to less than a week before the cycle start, a configuration is generally chosen on the basis of the "unconfirmed" core loading for that specific cycle.

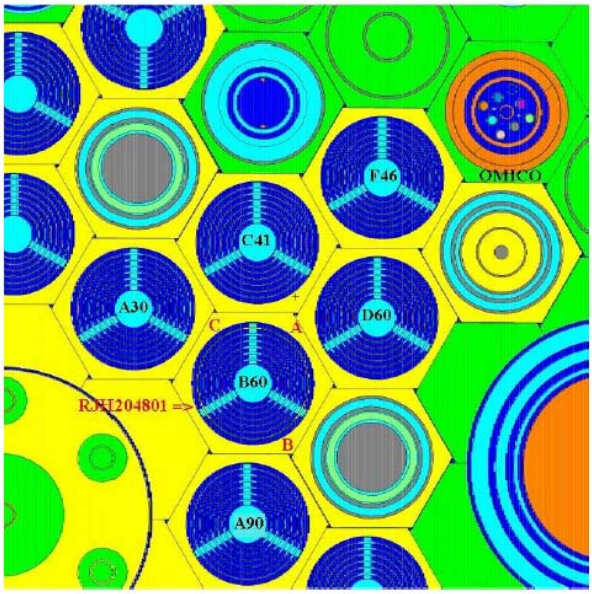

Figure 8: Core loading of BR2 for cycle 2005/4: detail of the neighbourhood of OMICO (top right of the figure)

Calculations with the "confirmed" core loading may then be performed *post-factum* and the thermal balance data are recalculated accordingly (if needed). Since the power distribution may vary considerably with control rod position, the following parameters are calculated for five different control rod elevations (400, 530, 650, 780 and 900 mm):

- the linear power (W/cm) due to gamma and neutron capture heating of the CALLISTO inner pressure tube
- the mean linear power (W/cm) of every fuel rod
- the maximum linear power (W/cm) of every fuel rod
- the total power (W) deposited in the upper and lower bundle (including the basket tube and the up streaming water
- the power (W) deposited in the down coming water.

These data are then incorporated in the software for the online thermal balance exploitation (INCA programme).

The power values in the structural parts are calculated as total power deposited in the specified volumes, regardless of their origin (neutron capture, prompt or delayed gammas from BR2 driver fuel or OMICO fissions). For the fuel segments, the fission events are calculated first and an effective energy per fission of 196 MeV (see also [13], Appendix 2,

§3.3) is attributed in order to obtain the linear power density. All values are normalized to the nominal reactor power.

Densities of fission events (axial profiles, calculated as fissions/cm) are calculated in segments of 21 mm for the non-instrumented rods and in segments of 15.3 mm for the instrumented rods. Fast (E > 1 MeV) neutron flux density distributions and neutron spectra are calculated for the purpose of fuel-performance calculations using the same full core model.

3.4.2.4 Online recording of irradiation history

The irradiation history (linear power versus time) is available for all fuel rods in digital format. The total burn-up for all rods, as obtained from an integration of the online data, is given in Table 7. For the non-instrumented rods, the online data are to be applied directly, but for the instrumented rods, the online recorded power history is to be corrected by the factors reported in Table 9. The appendix to Deliverable 8 [14] contains the condensed irradiation history as well as the correction factors in digital format.

Table 7: Online recorded burn-up for each rod and each irradiation cycle

	Instrumented rods (GWd/tHM)					
	A	B	C	G	H	I
2004_5	2.2	2.6	2.3	2.2	2.3	2.1
2005_1	1.9	2.2	1.8	1.6	1.7	1.5
2005_2a	0.0	0.0	0.0	0.0	0.0	0.0
2005_2b	2.2	2.6	2.2	1.9	2.0	1.8
2005_3	2.0	2.3	1.9	1.8	1.9	1.6
2005_4b	0.6	0.8	--------	0.5	0.6	0.5
Total	**8.8**	**10.5**	**8.3**	**8.0**	**8.5**	**7.5**

	Non-instrumented rods (GWd/tHM)					
	A	B	C	G	H	I
2004_5	2.0	2.3	2.0	1.9	2.0	1.8
2005_1	1.8	2.0	1.7	1.5	1.6	1.4
2005_2a	0.0	0.0	0.0	0.0	0.0	0.0
2005_2b	2.0	2.4	2.0	1.7	1.8	1.5
2005_3	2.0	2.3	2.0	1.8	1.9	1.6
2005_4b	0.6	0.7	0.6	0.5	0.6	0.5
2006_3	1.4	1.6	1.4	1.2	1.3	1.1
2006_4	2.5	3.0	2.5	2.7	3.0	2.5
Total	**12.4**	**14.2**	**12.2**	**11.4**	**12.2**	**10.4**

3.4.2.5 Off-line verification: gamma spectrometry reference

In Tables 8 and 9, the burn-up as determined by the gamma spectrometry analysis (results obtained in WP 5 [17-19]) is compared to the values obtained from the integration of the read-out of the thermal balance. The burn-up values are given in units GWd/tHM. The direct output of the gamma spectrometry is always given in fissions per initial heavy metal atom.

The transformation from energy to fissions uses an effective value of 196MeV/fission for all rods, value that is used for the transformation of the measured enthalpy increase (in the thermal balance) to the linear power in each of the fuel rods. When considering the results of Table 8 it is concluded that the integration of the online recordings agrees with the gamma spectrometric results within experimental margins (4%) for the non-instrumented rods, but for the instrumented rods, the online recording slightly differs from the gamma spectrometry results. The values agree within experimental margin (4%) for rod B, but for all other rods, the online recording slightly underestimates the value as given by gamma spectrometry.

Table 8: Gamma spectrometry results versus thermal balance results for the non-instrumented rods

NDT-1 campaign (after cycle 2004/5)						
	A	B	C	G	H	I
Rod average BU from gamma spectrometry (GWd/tHM)	2.00	2.25	1.99	1.90	2.04	1.79
Rod average BU, from thermal balance (GWd/tHM)	2.01	2.38	1.96	1.93	2.11	1.85
Ratio gamma spectrometric to thermal balance	100%	95%	101%	99%	97%	97%

NDT-2 campaign (after cycle 2005/4)						
	A	B	C	G	H	I
Rod average BU from gamma spectrometry (GWd/tHM)	8.72	9.55	8.45	7.72	8.02	6.98
Rod average BU, from thermal balance (GWd/tHM)	8.49	9.77	8.16	7.47	7.93	6.82
Ratio gamma spectrometric to thermal balance	103%	98%	104%	103%	101%	102%

NDT-3 campaign (after cycle 2006/4)						
	A	B	C	G	H	I
Rod average BU from gamma spectrometry (GWd/tHM)	12.93	14.12	12.65	11.79	12.48	10.71
Rod average BU (thermal balance, GWd/tHM)	12.45	14.35	12.12	11.44	12.25	10.43
Ratio gamma spectrometric to thermal balance	104%	98%	104%	103%	102%	103%

Table 9: Gamma-spectrometry results versus thermal-balance results for the instrumented rods. Due to leaching of Cs at the location of the defect, the value for rod C is not reliable. A lower limit of the correction value is 105%, but for correcting the irradiation history, the value deduced for rod A (110%) has been applied

Additional PIE campaign (after cycle 2005/4)						
	A	B	C	G	H	I
Rod average BU from gamma spectrometry (GWd/tHM)	9.7	10.8	n.a.	8.6	9.0	8.1
Rod average BU, from thermal balance (GWd/tHM)	8.8	10.5	8.3	8.0	8.5	7.5
Ratio gamma spectrometric to thermal balance	110%	102%	n.a. (>105%)	107%	106%	107%

3.4.2.6 Failure of instrumented pin C

On Tuesday 23 August 2005, instrumented rod C failed (Figure 9). The failure occurred during cycle 2005/3, which is the fourth irradiation cycle of the OMICO bundle. The cycle started on 29 July and the fuel was irradiated at power levels less than 300W/cm.

On 23 August 2005, at 8.36, the pressure transducer (PT) of rod C started to rise together with a sudden temperature increase from 1129 °C to 1172 °C[15]. As there were no physical conditions for the release of fission gas to occur, the rise of PT signal indicated malfunctioning of this fuel rod, with either a malfunctioning of the LVDT detector or a microscopic breach of the fuel cladding with ingress of coolant at 150 bar (the rod internal pressure is only 10 bar). Failure of an LVDT detector did already occur twice with the OMICO rods in the past and was never related to fuel rod failure. In both previous cases, the failure was related to a short circuit in the long instrument cables, and in one case, a repair could be made successfully.

Short circuiting the LVDT signal cables leads to a false reading of approximately 22 bars, while the true pressure remains at approximately 10 bar. During the event with the instrumented rod C on 23 August, the recording of the pressure transducer continued to rise to 45 bar reading, which corresponds to the maximum displacement of the ferritic core in the LVDT and this reading must be interpreted as fuel rod failure and not as LVDT cabling short circuit. This reading was recorded at 11.25, with a second jump in centreline temperature to about 1200 °C. Shortly after this event, recorder RIA371 indicated the presence of gamma activity in the bleed line of CALLISTO, with subsequent indications of activity in the surge tank and in the vent line of the surge tank (detectors RIA 424 and 425). The rise of the gamma activity is related to the release of volatile fission products from the fuel rod, which was confirmed by gamma spectrometry measurements of samples taken from the CALLISTO coolant. The activity of the ^{129}I isotope corresponds to 8kBq/ml, which is well above the threshold for shutdown of the reactor. The reactor was shut down at 21h.

In the shut-down period between cycle 2005/3 and 2005/4, pin C was successfully replaced by a dummy rod. During cycle 2005/4, a second fuel pin failure occurred with similar history. It was then decided to remove all the instrumented rods and to replace them by an

equivalent stainless steel piece having the same weight and leading to a similar flow pattern in the IPS 1 and to continue the irradiation for two more cycles with the non-instrumented rods only.

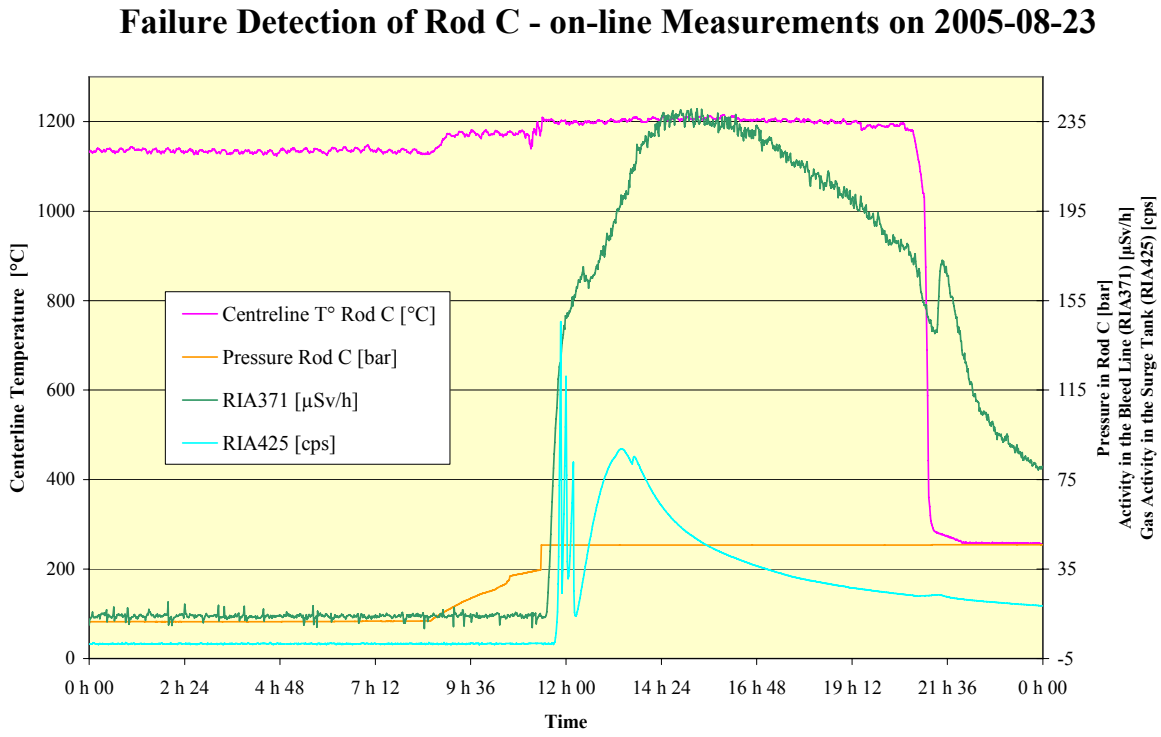

Figure 7: Online measurements of the failure of rod C

3.4.2.7 Reorientation of the irradiation scope after failure of the instrumented rods

During meeting M8 (December 2005), the options for continuation of the OMICO experiment were discussed. It was argued that given the good power analysis, the "thermal modelling" objective of OMICO was already met and that the "fission gas release" objective of OMICO can also be met with the non-instrumented rods only. The partners agreed to aim at a continuation of the irradiation experiment with the non-instrumented rods only.

This involved the removal of all instrumented rods and their replacement by an equivalent volume of stainless steel. With the modified structure, two irradiation cycles were performed with the non-instrumented pins only: one low power irradiation cycle (below the FGR threshold) for calibration of the modified structure and the second cycle at more elevated power (above the FGR threshold). A puncture of two rods (UO_2 rods A and C) will be performed after the third and final ND-PIE campaign (complementary PIE). The scientific objectives of the project shall in this way be met, but with a modified approach.

3.5 WP5 Post-irradiation investigations

3.5.1 Base analysis

From the start of the OMICO programme, several intermittent non-destructive PIE campaigns were defined on the non-instrumented rods. All campaigns contained gamma spectrometry, visual observation (Figure 10) and profilometry (Figures 11 and 12) and constitute the reports of Deliverable 10 [17-22].

1. A first campaign was defined after the first cycle, and this campaign focused primarily on the verification of weld condition (visual observation), and verification of the predicted power and online recorded power by gamma spectrometry. In addition, diameter measurements and eddy current measurements were performed as well.
    a. Visual examination revealed no visual damage or defects on any of the fuel rods, the cladding shows a homogeneous dark brown coloration. Special attention was paid to the aspect of the welds, but all welds are found to be in very good condition.
    b. Gamma spectrometry evaluation of power and burn-up on the basis of ^{140}Ba-^{140}La (short-living) and ^{137}Cs (long-living) isotope analysis gave a slightly different result (7% lower) than obtained from the online thermal balance reported initially for that cycle. A careful review of the online recording demonstrated that during that particular cycle (2004/5), a sudden change in recorded power was observed during the start-up. This was attributed to a change in thermal loss and the comparison of the axial heat loss calibration prior to cycle 2004/5 with all subsequent calibrations confirmed our understanding of the phenomenon as an artefact. The data set of the online power recording was therefore recalibrated using the calibration file of the subsequent cycle (2005/1). No further artefacts of this kind were observed.
    c. The axial power profile corresponds to the MCNP calculations within statistical error.

2. The second ND-PIE campaign was performed after the removal of all instrumented rods (after fifth irradiation cycle) and it had as main objective to secure the non-instrumented pins and to search for failure causes of the instrumented pins.
    a. None of the non-instrumented pins shows degradation; PCMI is not present (creep down is not completed yet). It could be concluded that irradiation can be continued with the non-instrumented rods.
    b. Regarding the instrumented pin C, profilometry showed swelling of one of the end pellets (Hf_2O_3) and cladding defects at three positions. The Eddy Current scans confirmed the cladding defects as non-penetrating (once) and penetrating (twice). The penetrating defects can easily be identified visually and are located close to the top end plug (spring position) and at approximately 2/3 height. The location of one non-penetrating defect is at the tip of the central thermocouple (TC).
    c. The fact that all non-instrumented rods are intact and show no sign of degradation proves that fuel manufacturing can be ruled out as primary cause for failures. Definitive conclusions on the failure causes for the instrumented rods will require further investigations, but the location of non-penetrating defects at the TC tip position and swelling of the Hf_2O_3 end pellet located also

at the TC side, are indicative for either TC failure or failure of the TC feed-through (end plug failure).

d. The second gamma spectrometry campaign confirms the findings of the first campaign: when using the correct axial heat loss calibration data, the online recorded values for linear power are in agreement with the burn-up value as derived from gamma spectrometry.

3. The non-destructive "base package" PIE of the third campaign completes the two previous campaigns on the non-instrumented rods. It focused on the surface appearance, analysis of creep and final confirmation of the burn-up by gamma spectrometry.
    a. Visual observation confirms the findings of the previous campaigns: i.e. no severe oxidation is going on, and the welds remain in correct condition.
    b. Clad creep continues slowly but steadily, and with the very limited creep (less than 10μm for all rods at the level of the fuel stack); the pellet-clad gap should still be open. The rods all show quite substantial ovality (up to 30μm).
    c. Gamma spectrometry confirms the online power recording for the non-instrumented rods. The axial variation (shape factor) as calculated by MCNP is also confirmed.

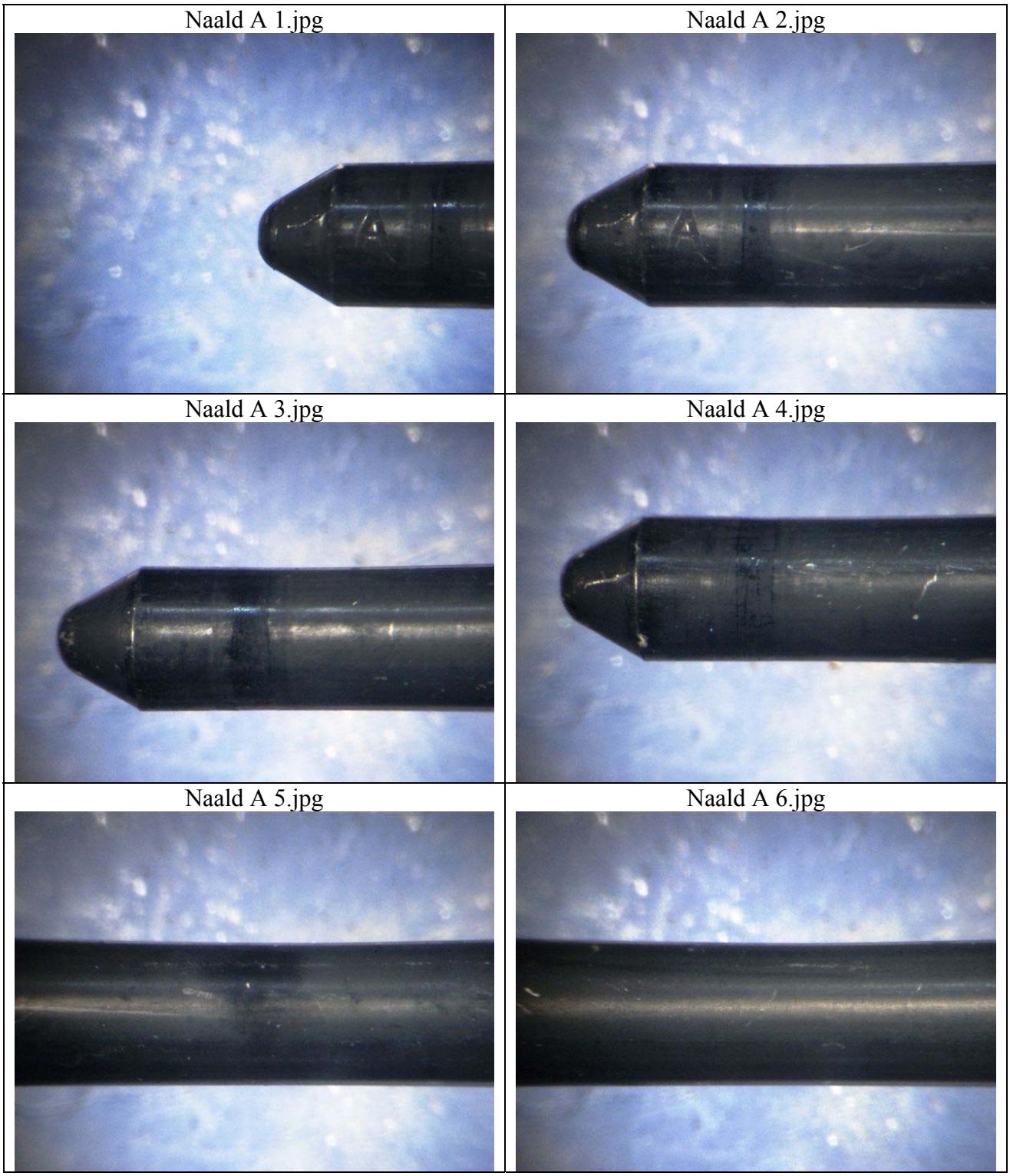

Figure 8: Example of visual observation results for rod A after seventh cycle: dark, non-lustrous oxide layer is formed

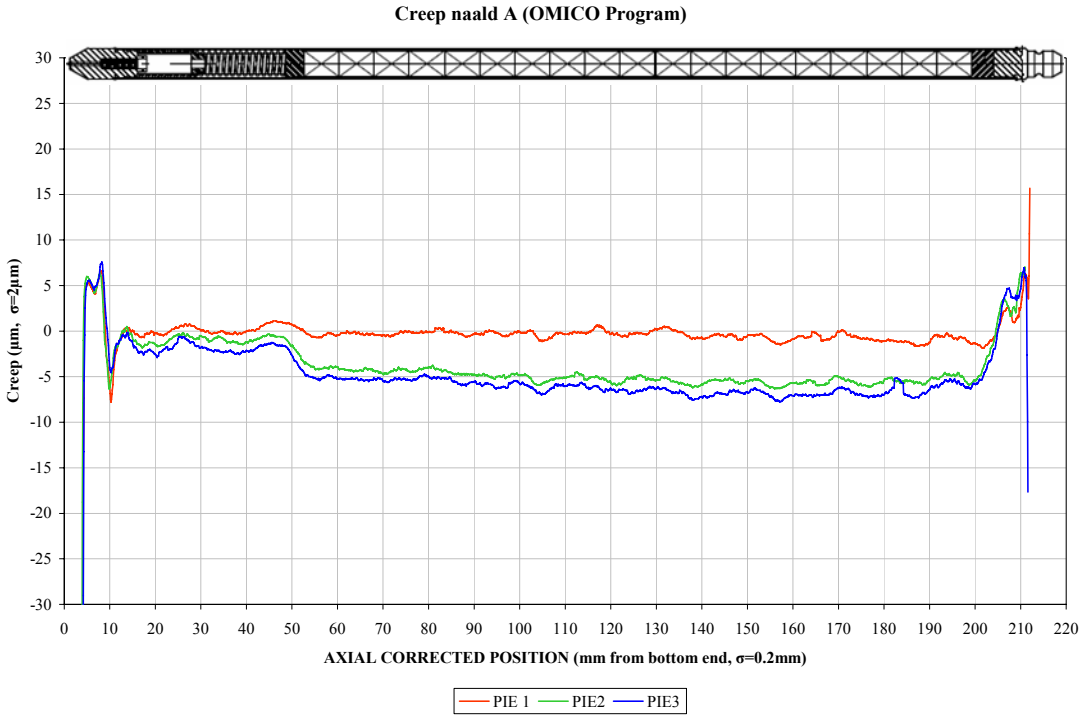

Figure 9: Creep profile of rod A. At the level of the spring, creep is approximately 3µm. At the level of the fuel stack, creep is between 5 and 7µm. Similar values are observed for the other rods

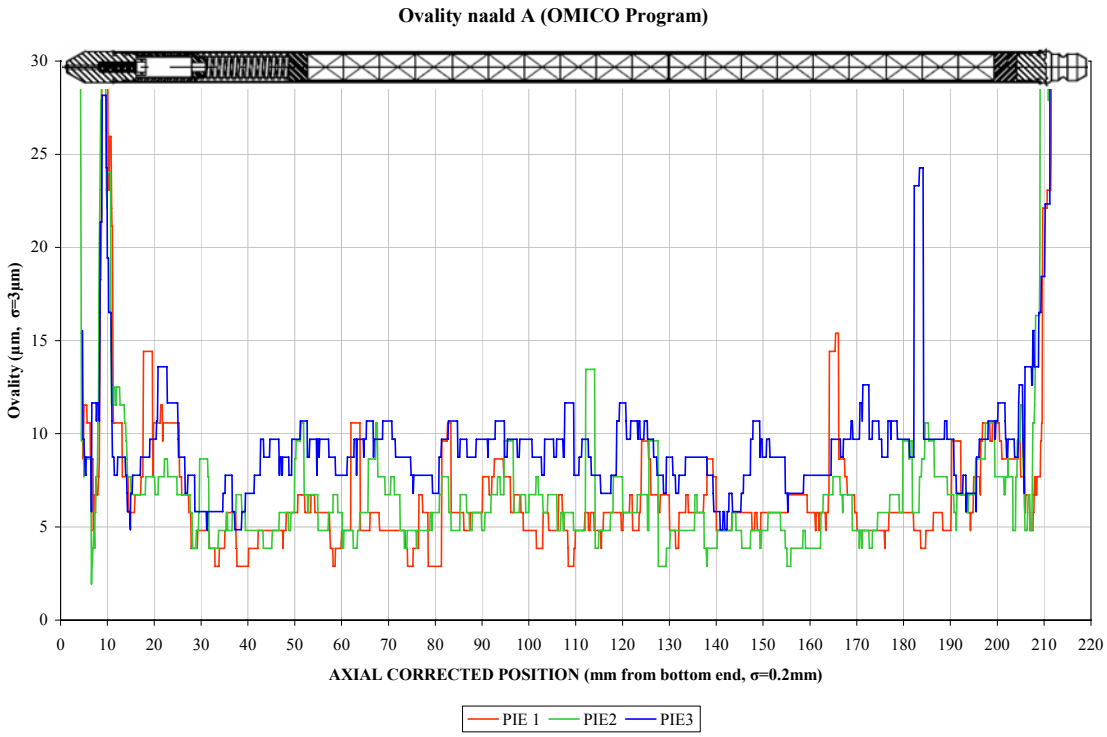

Figure 10: Ovality analysis of rod A: locally, ovality values of 25µm are found. The other rods also show ovality between 10 and 30µm

3.5.2 Complementary PIE

The problems encountered with the failure of the instrumented rods at the end of the fifth cycle and the important differences between calculated and measured centreline temperatures, led us to define a complementary PIE programme, Deliverable 12b [23-26].

Destructive tests on two UO_2 rods and one MOX rod:
- optical microscopy in as-polished and grain etched state of the two UO_2 and one MOX
- EPMA to recover the fissile distribution (only in the heterogeneous MOX and UO_2 fuels (direct Pu maps in MOX, indirect approach in heterogeneous UO_2).

Destructive tests:
- puncture test of non-instrumented rods A and C
- optical microscopy in as-polished and grain etched state of the two UO_2 and one MOX
- EPMA to recover the fissile distribution (only in the heterogeneous MOX and UO_2 fuels (direct Pu maps in MOX, indirect FP maps in heterogeneous UO_2).

3.5.2.1 Complementary non-destructive PIE on the instrumented rods

The complementary ND-PIE [23, 24] on the instrumented rods is focused on investigating the discrepancy between measured temperature data and calculated temperature data, as discussed on the OMICO Progress Meeting M9. The measured centreline temperature was found to be much higher than expected on the basis of the reported linear power, especially for the UO_2 fuel rods. The investigations should also bring further elements to find the cause of failure of rods C and G.

The complementary ND-PIE consisted of:

- Visual examination to evaluate the surface appearance of the cladding and the status of the bottom, top plug and seal weld.
- Diameter measurement along the axis of the fuel rod (i.e. profilometry, Figure 11 and Figure 12) to evaluate possible diametrical variations induced by creep and/or pellet-clad interactions. Also the ovality of the cladding is measured. Creep out, hence less thermal conductivity as the fuel-cladding gap increases, could be an indicator for the discrepancy in centreline temperature.
- Outer oxide thickness measurements along the axis of the fuel rod, to check for any unexpected thick oxide layer, which could explain a lower thermal conductivity of the cladding which again would result in higher centreline temperatures.
- Clad integrity evaluation by eddy current to trace any unusual deformation or damage.
- Gamma-activity measurements to determine the axial burn-up profile over the fuel stack and look for evidence of Cs-migration (Figure 15).

The following results were obtained:

- For fuel rod A, B, H and I, no defects or damages could be identified due to irradiation.
- Profilometry measurements show a maximum creep down of -8µm, comparable to the non-instrumented rods. On the contrary, the ovalities are larger compared to the non-instrumented rods, especially for fuel rods A and C, up to 80µm in the high power zone.

For fuel rod A the profilometry points out in the direction of pellet-clad interaction above the hollow pellets, which is confirmed by the presence of artefacts in the oxide thickness measurements. For all fuel rods strong cladding interaction of the hollow YSH-pellet was measured.

– The overall thickness of the oxide layer is less than 5µm, except for fuel rod A and G, which shows local axial oxidation up to about 25µm extending azimuthally over about ¼ of the cladding circumference.
– No evidence for excessive creep out or cladding oxidation could be found to explain the discrepancy between measured and calculated temperatures.
– Fuel rod C has three defect in the cladding:
  - Defect 1: internal orientated at 73mm from the bottom reference at the level of the thermocouple tip
  - Defect 2: through hole at 220 mm from bottom reference
  - Defect 3: through hole at 301mm from bottom reference at the level of the plug insert
– Fuel rod G has three anomalies which should be investigated destructively in order to classify it as a defect:
  - Anomaly 1: in seal weld
  - Anomaly 2: in the centre of the top plug weld "small crack" and "bulge"
  - Anomaly 3: small unidentified eddy current signal at 222.4mm from bottom reference
– The gamma spectrometry on the instrumented rods indeed found that for the non-instrumented rods the online values need to be corrected (see Table 9): rods A and C by 10%, rods G, H and I by 7%. For rod B the difference between the two methods is within experimental error margins. The data package exchanged in the course of the project must be corrected by these values.
– The form factor was initially derived from the MCNP calculations. It is known that the form factor varies with control rod position, but the actual variation is difficult to assess due to the inherent conflict between precision, resolution and accuracy in the adopted MCNP method. The gamma spectrometric analyses confirm that the average form factor is correctly computed (Figure 13). It is therefore decided to adopt a fixed axial form factor for the benchmark calculations. Variations of the form factor with control rod position will have a slight influence at the end of each cycle, when control rods are at their highest position.

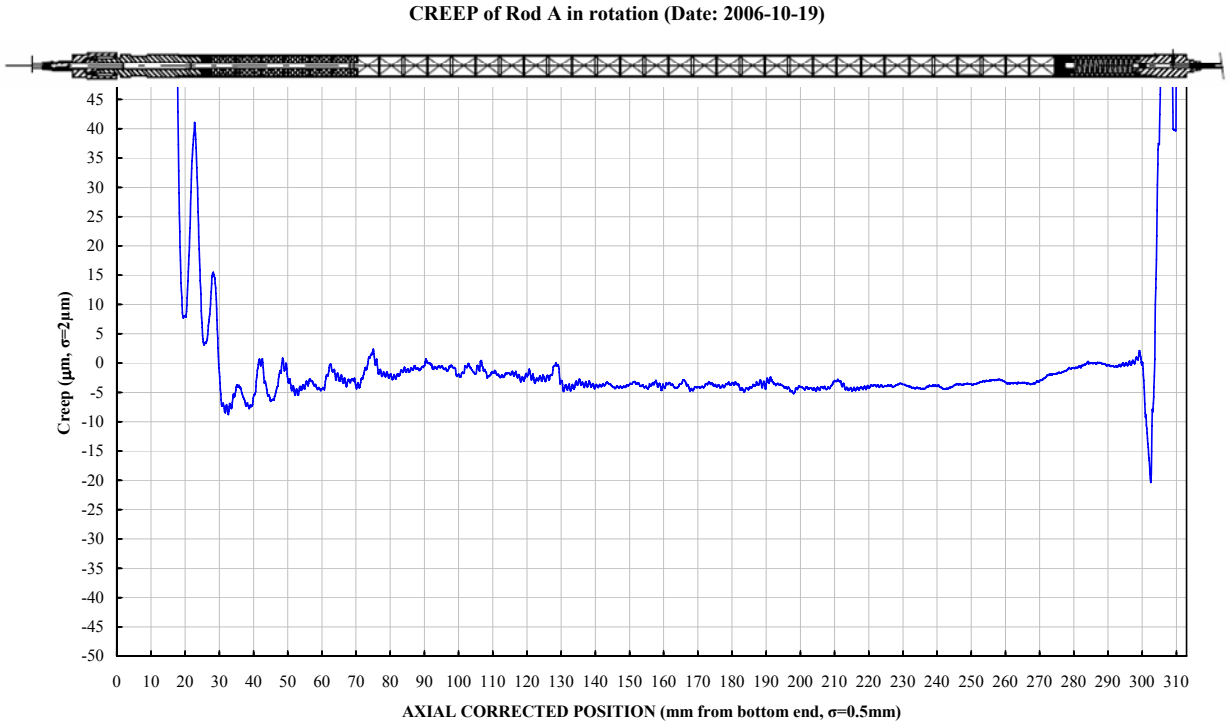

Figure 11: Creep profile of instrumented rod A. The zero value of creep is defined at the level of the spring. Maximum creep down is about 8µm (with respect to the diameter value at spring level). These values would be compared with values observed in Figure 11

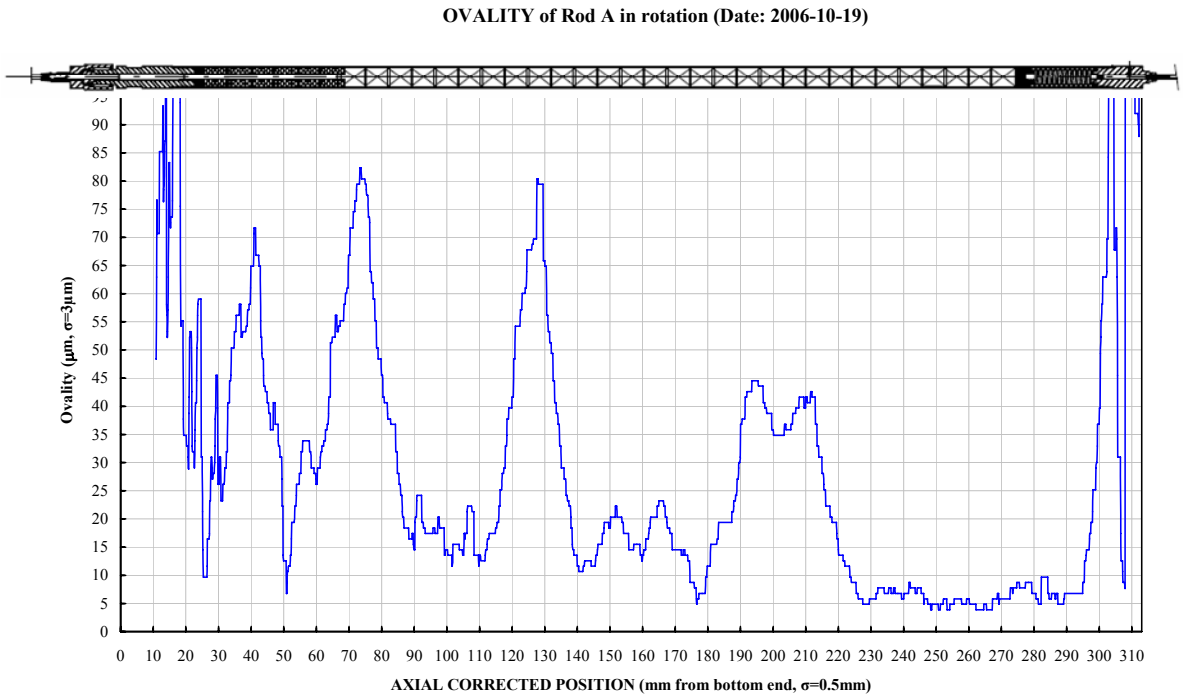

Figure 12: The ovality observed on instrumented rod A is much more important than found for the non-instrumented rods (see Figure 12). The same is also observed for the other instrumented rods

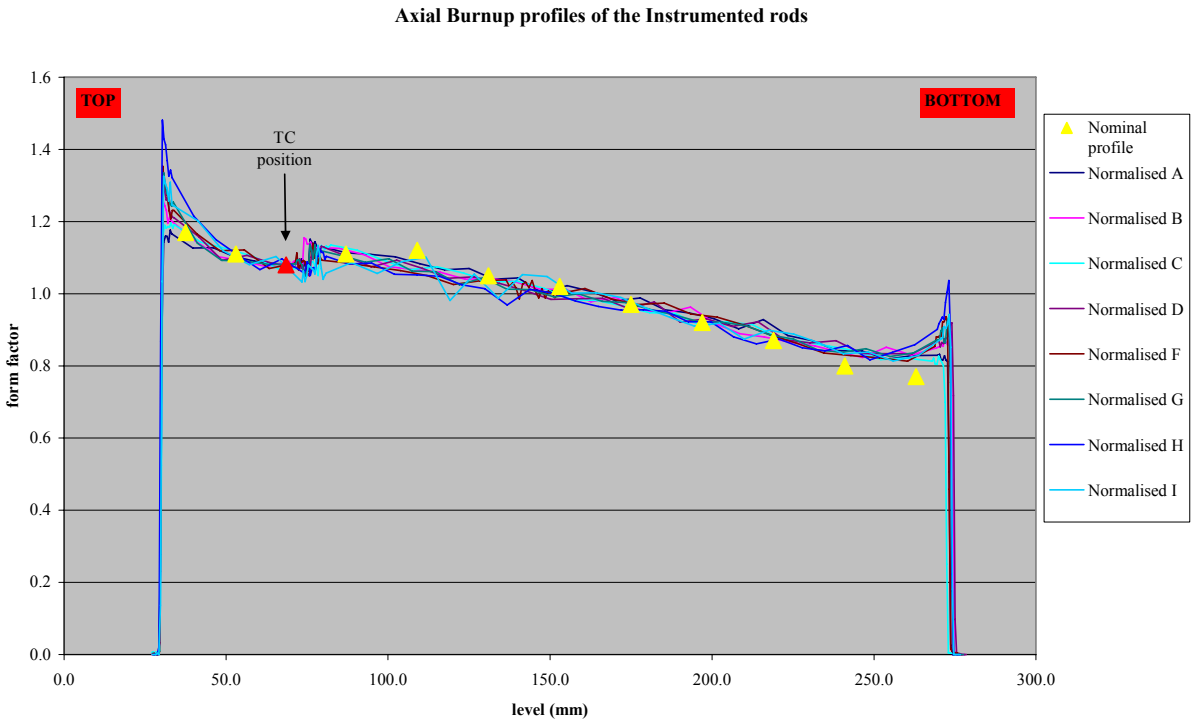

Figure 13: The normalised burn-up profiles confirm that the applied nominal profile (MCNP) is correct at the TC level and that for purposes of temperature calculations, the adopted nominal profile is to be maintained

3.5.2.2 Complementary destructive PIE

Microscopic and spectroscopic examinations of pellets from two instrumented UO_2 rods (A, C) and one instrumented MOX rod (I) from the OMICO irradiation campaign were done in as-polished condition [25]. The optical microscopy (OM) examination was oriented to investigate thermal barriers such as gap size, porosity, fracture pattern, relocation. It also provides information on microstructure differences between periphery and centre and densification of the fuel. The electron probe microanalysis (EPMA) investigations were performed to recover the distribution of the fissile isotopes in the C and I samples. Sampling is made from the instrumented rods, and samples are taken at the top of the solid fuel part (i.e. at high power position).

Optical microscopy observations can be summarised as follows:

- All three fuels show a fairly typical crack pattern, with open gap (Figure 16). In the sample taken from fuel A, the onset of circumferential cracking is observed, while for the two other fuels, only radial cracks are found. Quantitative observations are reported in Table 10.
- The outer clad corrosion layer is thin, as was also observed from the non-destructive testing. The destructive testing failed to confirm the NDT observation on rod A of locally increased outer oxide layers (see § 3.5.2.1). Careful examination of the sampling positions proved that the sample taken for destructive testing was indeed between two positions of increased outer oxide thickness.

- It is surprising to find inner oxide corrosion of the cladding for rods C and I, which is normally not expected as long as the gap is open.
- Cold gap size is measured at 6° interval and averaged. The reported value is the radial gap size. It amounts to ~ 45µm for both rods A and I, and ~30µm for rod C. In all cases, such cold gap size is expected with minimal creep as observed from the non-destructive testing and confirms that the gap was still open, also in hot conditions. The important difference between the gap of rods A and I with the value observed for rod C is surprising, but is correlated with and can be explained as a result of the development of a-typical porosity in fuel C.
- The porosity observed in the different fuels is indeed a-typical for both UO_2 fuels. Only in fuel I (heterogeneous MOX), the porosity is in accordance with the expected evolution of a denser fuel towards the centre of the pellet. For fuel A, there is no evolution, while for fuel C, the porosity increases from a fairly high value (9%) at periphery to 21% at the fuel centre. In view of the irradiation history, such evolution is not expected: fission gas release should not have occurred at the relatively low linear powers and burn-up.

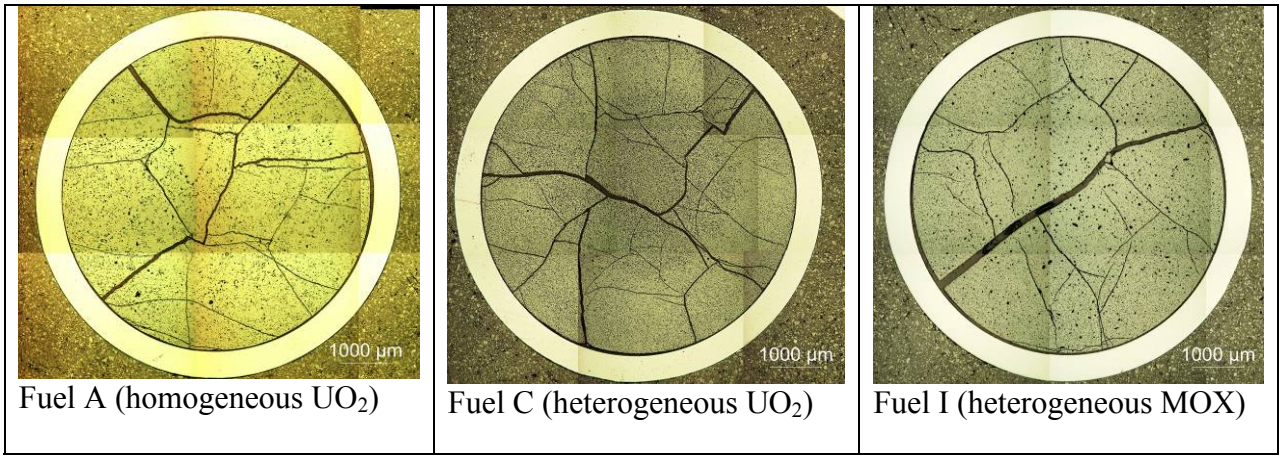

Fuel A (homogeneous UO_2) | Fuel C (heterogeneous UO_2) | Fuel I (heterogeneous MOX)

Figure 16: Macro image of the cross section of the three fuel samples subject to optical microscopy

Table 10: Cold-gap size, corrosion layer thickness and porosity

	A	*C*	*I*
	Radial gap size		
Cold gap (µm)	**43.9**	**30.5**	**45.1**
	Corrosion		
Outer oxide (µm)	**3.1**	**2.9**	**2.5**
Inner oxide (µm)	**0**	**6.8**	**5.4**
	Porosity		
Porosity (periphery)	**5.2%**	**8.3%**	**8.9%**
Porosity (mid-radius)	**6.6%**	**10.2%**	**7.2%**
Porosity (centre)	**6.8%**	**20.8%**	**4.8%**

The EPMA observations can be summarised as follows:

- For the heterogeneous MOX sample (fuel I), X-ray mappings of the fissile element distribution can be made in the conventional way, i.e. by mapping the plutonium signal (Figure 17). Maps were made at periphery, mid-radius and centre, but little or no variation was observed in the fissile isotope distribution on going from periphery to centre.
- For the heterogeneous UO_2 sample, elemental analysis can of course not distinguish between ^{235}U and ^{238}U, and one has to rely upon the variation of the fission product distribution to recover the fissile isotope distribution indirectly. Since the concentration of fission products is too low for 2D image recording (X-ray mapping), X-ray intensities have been measured by defining a line scan from periphery to centre for the elements oxygen, uranium, neodymium and molybdenum. A dwell time of 60 s and beam intensity of 150nA were required because of the low concentrations of the fission products (Nd, Mo). The results of this line scan are given in Figure 18. At pellet periphery, one clearly observes the heterogeneity of the Nd and Mo signals which are highly correlated between each other. Towards the centre, the Nd signal clearly becomes flatter, and the Mo signal is more peaked. A more homogeneous Nd distribution indicates rapid in-pile homogenisation of fissile and fertile isotopes. The peaking of the Mo signal indicates formation of five metal particles.

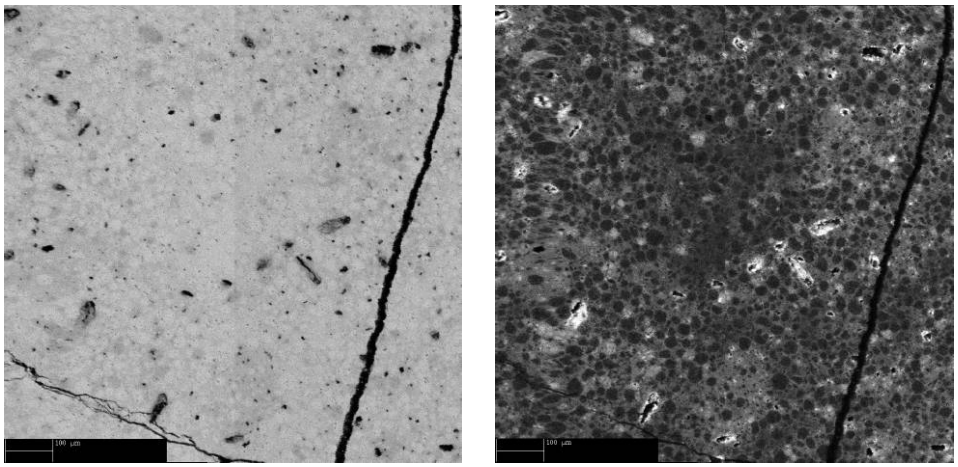

U Mα **Pu Mβ**

Figure 17: Uranium and plutonium mapping of fuel I. Highly enriched Pu zones seem to have the tendency to break out, most probably during sample preparation. Interdiffusion zones develop in accordance with the known properties of the diluting powder (TU2)

0 µm

1000 µm

Periphery

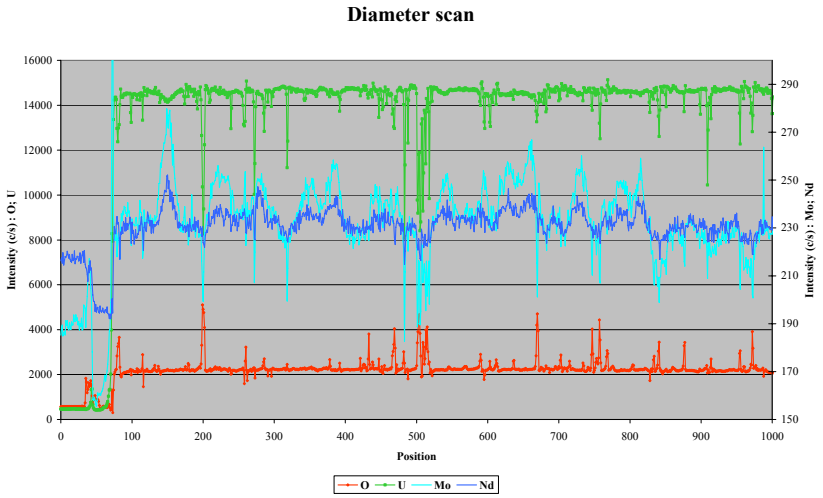

1000 µm

2000 µm

Mid radius

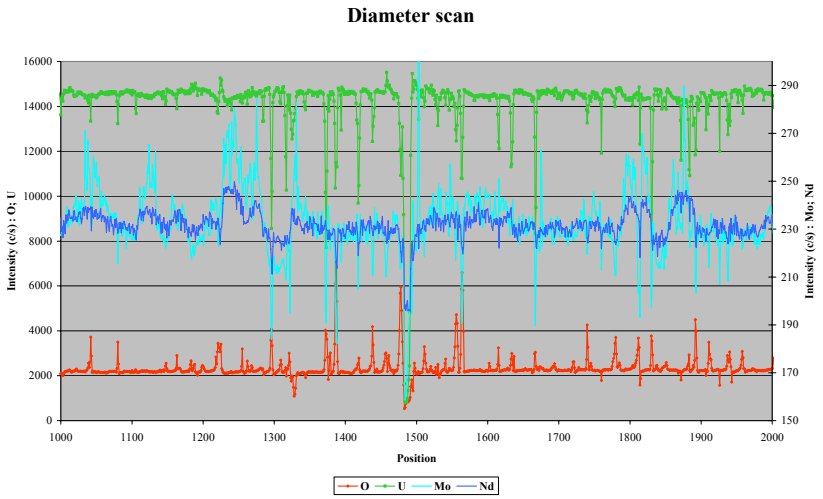

2000 µm

3200 µm

Centre

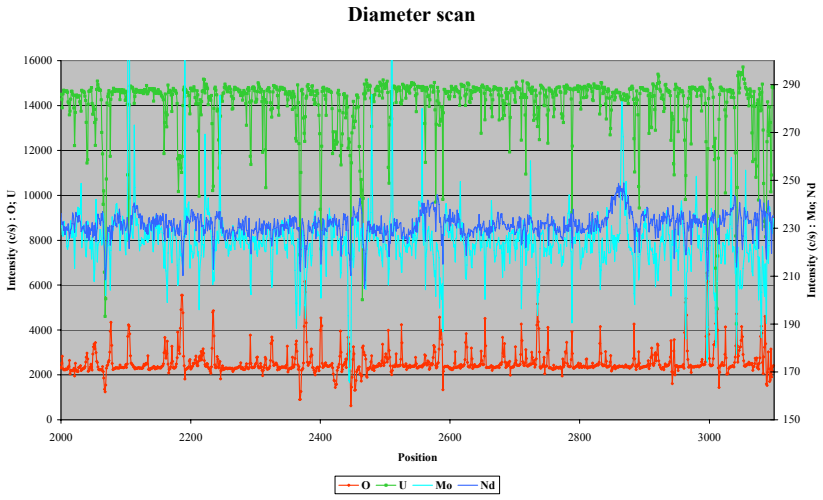

Figure 18: Line scans (U, O, Mo and Nd) on fuel C. The heterogeneous distribution of both Nd and Mo signals are clearly observed at pellet periphery. Towards the centre, the Nd signal becomes much flatter and the Mo signal is less correlated with the Nd signal, probably due to the clustering of Mo in five-metal particles

3.5.2.3 Puncture results

In order to obtain results on fission gas release, even though the instrumented rods failed before gas release was measured, it was decided in meeting M8 to define a special irradiation cycle at more elevated power and to puncture two rods (rods A and C) [26].

The non-instrumented OMICO fuel rods contain only 45g of nuclear fuel. The amount of produced fission products hence is minute, and the mass spectrometry had to be recalibrated on low pressures. Validation experiments were conducted prior to the OMICO analyses to assess the mass spectrometric results for samples with a low inlet pressure (~ 10 mbar instead of 500mbar). Several test ampoules were made containing a gaseous Kr/Xe mixture with different pressures. Comparison of the obtained values showed that the difference between the high and low pressure ampoules stays within the uncertainty of the measurement.

The puncture results are given in Table 11.

Table 11 Fission gas release of rods A and C

	Rod A			Rod C		
Xe release (cm^3)	0.0146	±	0.0029	0.0257	±	0.0052
Kr release (cm^3)	0.0024	±	0.0010	0.0043	±	0.0017
FGR release (cm^3)	0.0170	±	0.0031	0.0300	±	0.0054
FGR release (%)	0.12 %	±	0.02%	0.21%	±	0.04%

3.6 WP6 Code benchmarking and model development

3.6.1 Radial power profile in $(Th,Pu)O_2$ fuel pins and comparison to UO_2 and MOX

A method for full assessment of the spatial distribution of resonance capture in thorium-plutonium oxide fuel pins subject to neutron irradiation in thermal reactor conditions has been developed and reported as Deliverable 4 [27]. The method uses evaluated data libraries for Breit-Wigner resonance parameters. Based on evaluated resonance parameters a data file specifically oriented on the treatment of spatial resonance self-shielding is then produced. The Doppler effect is modelled in an analytical way for a wide range of temperatures (0 to 3500 K). The computation method of the resonance self-shielding was optimised with respect to limitations imposed by fuel-performance codes. Results for deposited energy are given in Figure 19.

Starting with the general neutron absorption probability forms for narrow resonances, analytical closed form expressions describing neutron absorption in the resolved resonance energy region were obtained. Full modelling of resonance absorption was performed assuming heterogeneous arrangement of absorbing fuel rods, i.e. for rods in a lattice. The

practical use of Bogard's method for fuel-performance modelling was illustrated and confirmed. His method is one of the key parts of the methodology.

The balance equations for energy release in binary fissions have been determined for all nuclei that are to be considered in the context of thorium, thorium-uranium and thorium-plutonium fuels for thermal reactor applications.

While the energy release part can be effectively modelled in a practical way, the integration in a fuel-performance code of the energy deposition would demand too much computation resources for a direct assessment.

It must be mentioned that after six decades of research on nuclear fuels and minor actinides standard libraries are still incomplete and are not fully consistent. Almost half of the heavy metal nuclei that must be taken into account in fuel-performance codes are not provided with evaluated data for basic neutronic properties. Discrepancies between major "standard" libraries make particular selections difficult. As a consequence, fuel-performance models for energy balance and for treatment of resonance self-shielding must reserve options and resources for all "standard" libraries.

Recently published theoretical works in the field of energy release and deposit in binary fissions along with new mass formulas and latest equations of state for dense nuclear matter at finite temperatures set a new basis for assessment of the thorium fuel cycle. A deeper assessment is recommended, especially in view of a growing industrial interest of the thorium fuel cycle.

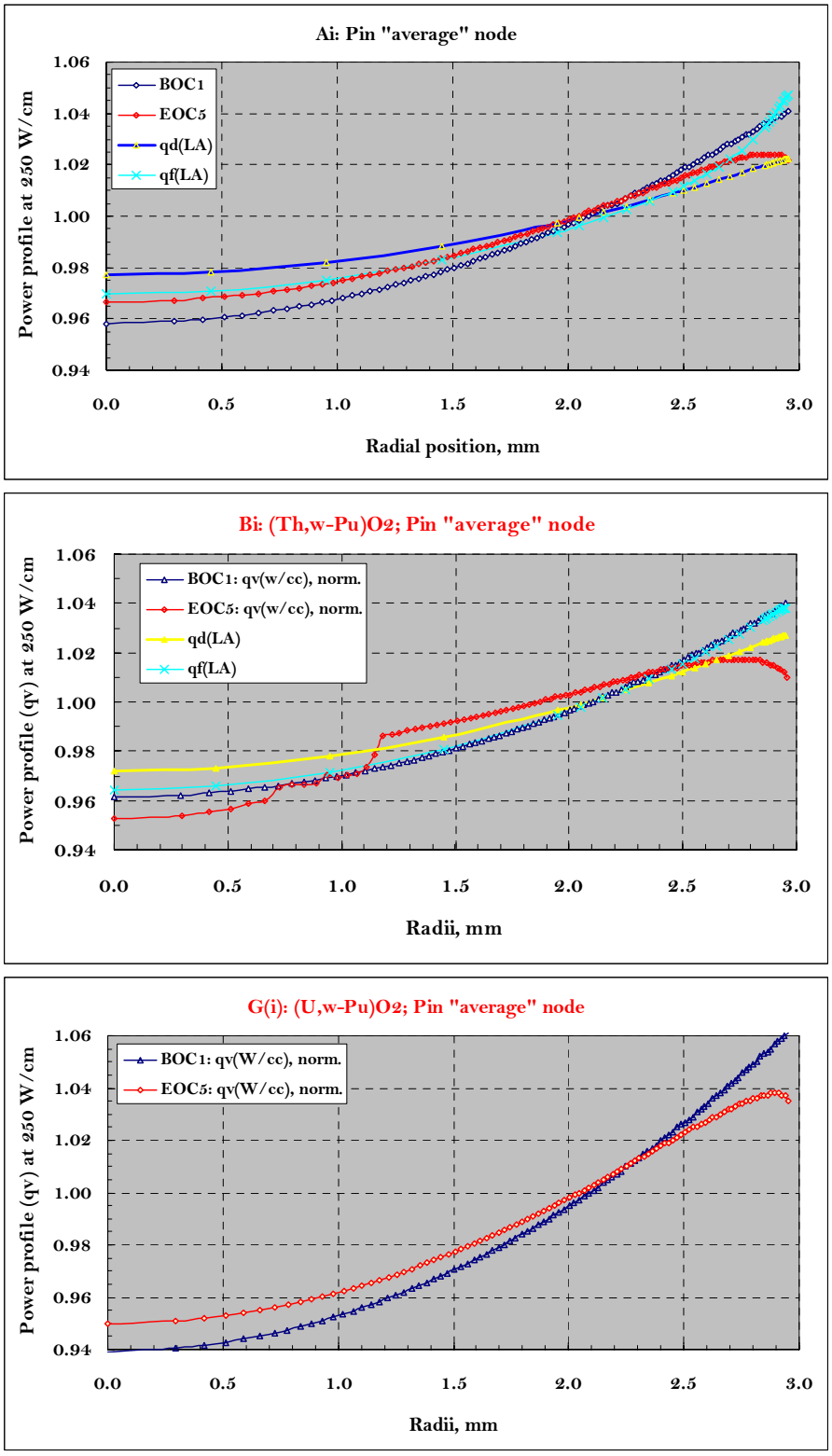

Figure 19: Deposited energy (W/cc) at BOL (BOC1) and EOL (EOC5) for the three homogeneous fuels: A UO_2, B (Th, Pu)O_2 and G (U, Pu)O_2. The BOL and EOL graphs are calculated taking densification and local temperature into account (swelling at centre of B, the q_d plots (deposited energy) which are added for UO_2 and Th, PuO_2 show calculated profiles obtained without taking the solid state effects into account; q_f plots show the fission profiles, which could be compared with experimental results from local fission product profiles, to be obtained from SIMS or EPMA measurements

3.6.2 Code benchmarking results

In the OMICO project three fuel-performance codes (MACROS, COPERNIC and TRANSURANUS) have been applied to simulate the thermo-mechanical behaviour of the instrumented as well as the non-instrumented fuel rod segments (Deliverable 11, [28], Figures 20 and 21). For the UO_2 and the $(U,Pu)O_2$ rods, the total spread between code predictions is in the order of 100 K, and such performance is comparable to the spread obtained in code verification exercises for standard UO_2 and MOX fuel. For the instrumented segments C_i (UO_2) and I_i $(U,Pu)O_2$ the spread reaches up to 150 K. In rod C, this can be understood on the basis of the development of high levels of porosity (see § 3.5.2.2), the cause of which is not understood at the moment.

The experimentally observed trend in fuel centre temperatures is simulated by the MACROS code, but is not immediately reproduced by the COPERNIC or by the TRANSURANUS code. The measured fuel temperatures in UO_2 and $(U,Pu)O_2$ can be simulated satisfactorily by COPERNIC in the first cycle. In the next cycles, the observed trend could be approached by a modification of the COPERNIC relocation model. For TRANSURANUS, the measured fuel temperatures in UO_2 and $(U,Pu)O_2$ can, be simulated satisfactorily by applying two different values for the fuel porosity: The pre-characterisation values on one hand, and an upper estimate from the PIE results (10%TD) on the other hand.

For $(Th,Pu)O_2$ the spread between code predictions (MACROS and COPERNIC) is in the order of 350 K, in some phases up to 400 K. A thorough analysis (including sensitivity tests) is required for clarifying the contributions of the different sub-models, such as the material properties and the radial power profile. The predictions of fission gas release are for the time being very tentative.

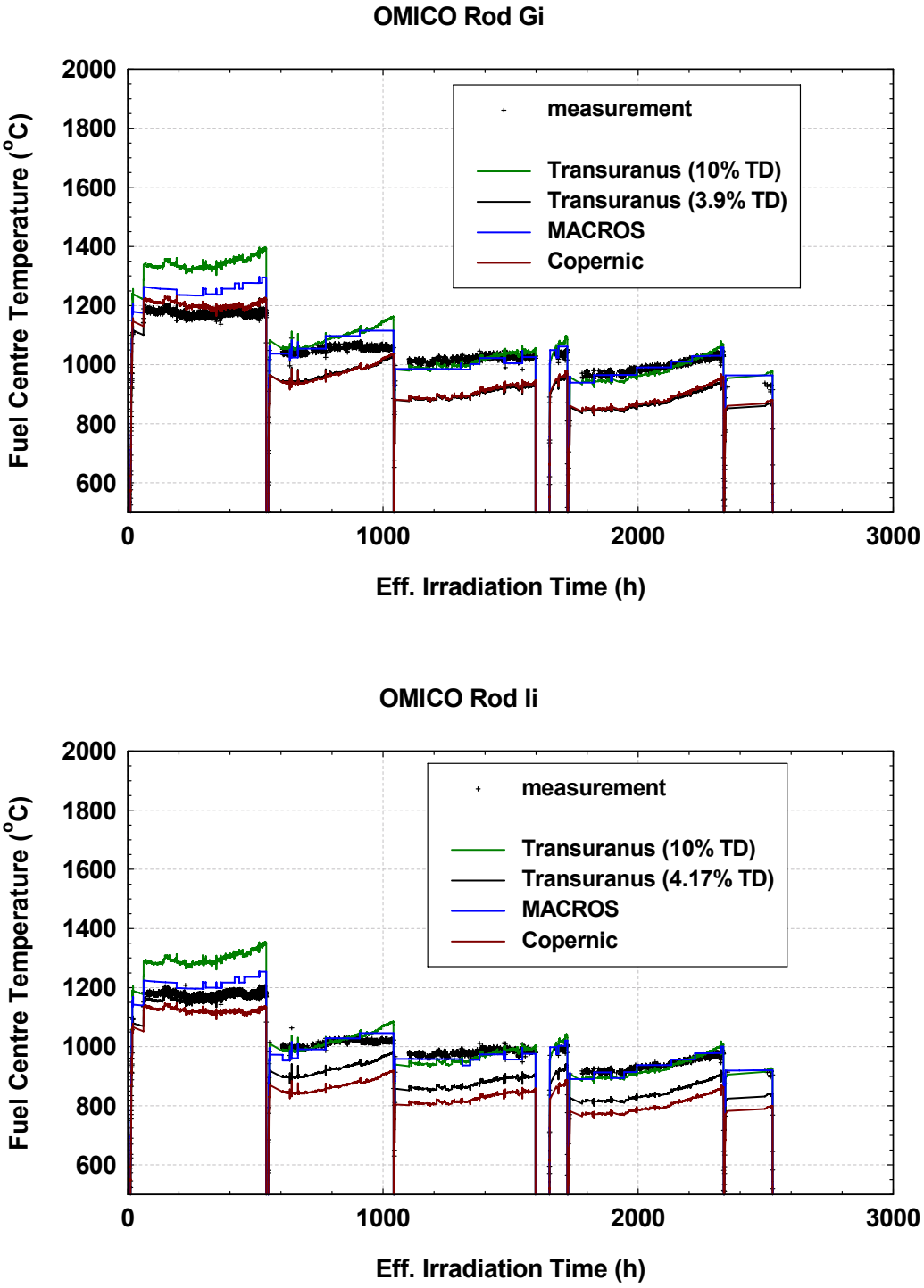

Figure 20: Experimental versus calculated centreline temperature for both $(U,Pu)O_2$ MOX rods as a function of time. For one of the codes (TRANSURANUS), two different options for porosity were tested and are reproduced

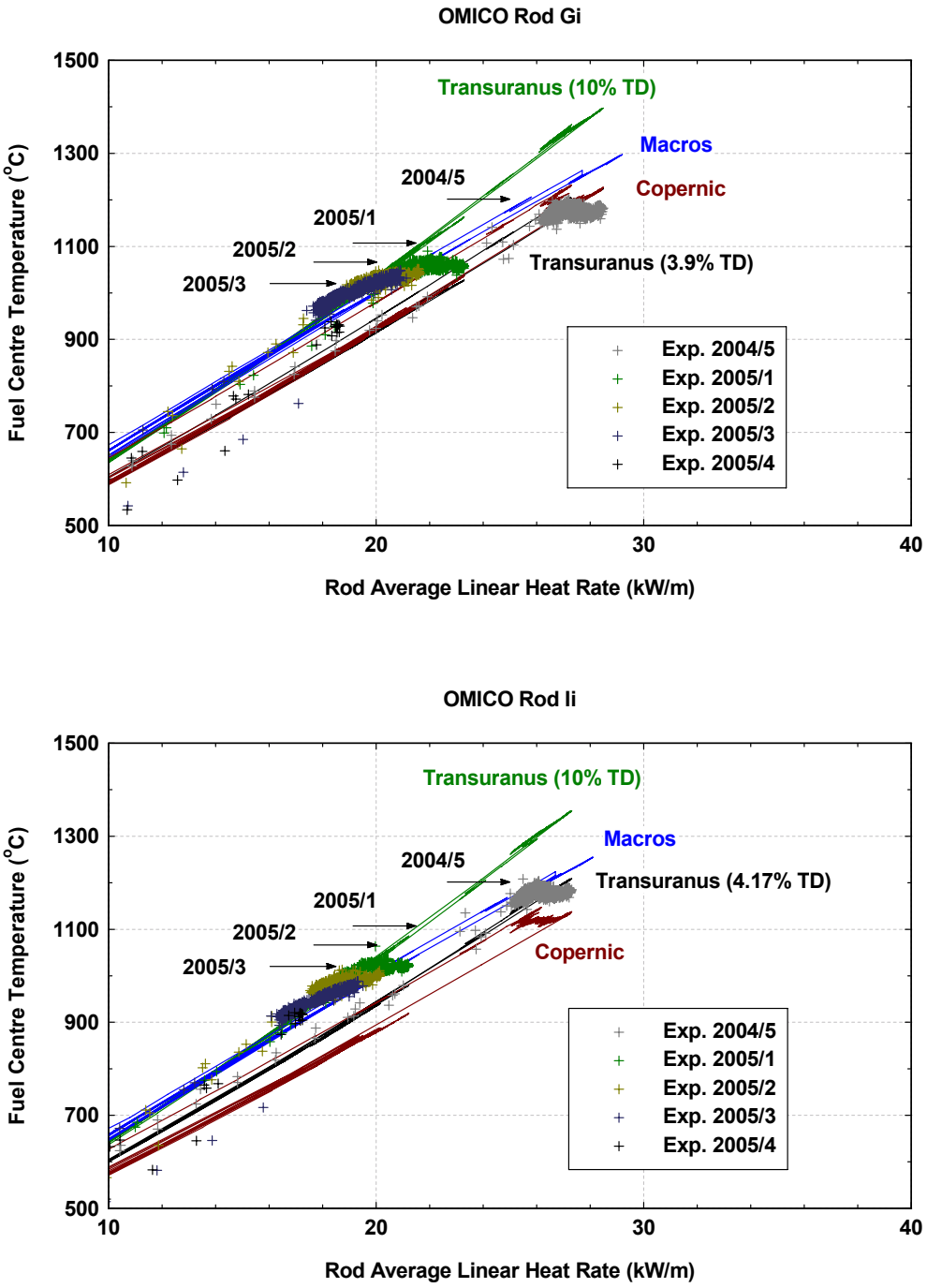

Figure 21: Calculated versus linear power compared to experimental centreline temperatures versus linear power. Similar as in Figure 20, for the TRANSURANUS code, two options for total porosity are calculated

4 Project achievements

The project OMICO incorporated several challenging objectives on nuclear fuels, requiring technological developments in various areas. The complexity of some of these technological developments was initially overlooked and/or their extent was underestimated. This situation led to substantially higher expenses at the research institutes JRC/ITU for manufacturing and SCK•CEN for irradiation (approximately 50 % additional costs paid from the own budget of the respective research institutes) than originally foreseen and a substantial delay of the project (66 months instead of the original estimate of 36 months).

Major causes for the delay and additional costs were related to:

- Fuel fabrication capacity at ITU was not available at the scheduled start of the fabrication campaign due to technical problems with other fabrications (MICROMOX).
- The geometric complexity of the fuel assembly necessitated a three-dimensional approach for neutronic calculations, the qualification of which was more time-consuming than expected.
- The manufacturing of instrumented and non-instrumented rods required several welding installations, and the qualification of corrosion resistance caused in total twelve months of delay, which was totally unforeseen.
- Pin failure caused substantial additional costs in reactor operation since the pressurised-water loop CALLISTO may not be operated with failed fuel pins. Fuel pin failure inevitably results in the interruption of the operation, reactor shutdown and removal of the failed pin. As a result, all other experiments, radio-isotope production etc. are affected by the fuel pin failures.

Despite its difficulties, OMICO did achieve important successes as well:

- The experimental OMICO assembly had to be calculated in a three-dimensional approach. At the time of start of the OMICO project, 3D Monte Carlo calculations were not yet established for the complex core of the BR2 reactor. The thorough cross-checks with the conventional 2D approach, comparison with reference programmes and the irradiation of a dummy assembly contributed to the confidence in the MCNP modelling of complex experiments in the BR2 reactor, and are today common practice.
- Fuel manufacturing to tight LWR specifications demonstrated once again ITU's key role as an independent experimental fuel manufacturer in Europe, and the OMICO programme has extended the core competence of this laboratory to heterogeneous $(Th,Pu)O_2$ and UO_2 fuels.
- The thermal diffusivity analysis was a first-of-its-kind for $(Th,Pu)O_2$. It was performed for different Pu contents, thereby filling a knowledge gap open for many decades and settling a number of debates on this parameter.
- The in-pile modifications to the CALLISTO loop, and especially the instrument feed-through system, are copied to other experiments. The search for a flexible and reliable solution for high-pressure, high-temperature feed-through of a large number of cables has been a technological axis of development in SCK•CEN for several years. The design developed for OMICO was a major breakthrough.

- The combined use of self-powered neutron detectors with the long-established thermal balance methods improved the reliability of power determination, which is crucial to all fuel experiments. Together with the MCNP approach and qualified gamma spectrometry methods, the accuracy and precision of the linear power determination has improved considerably.
- In terms of fuel-performance data, the OMICO experiment fully achieved the goals with respect to the acquisition of thermal data (power versus centreline temperature data-set).
- Regarding the fission gas release, the unfortunate loss of the instrumented rods after five cycles didn't allow us to address the dynamic evolution of fission gas release through online measurements. The definition of two dedicated cycles on the non-instrumented rods, one of which contained a mild transient, allowed recovering in part the objective of fission gas release.
- Non-destructive post-irradiation examinations successfully complemented the in-pile data on power determination. The creep data were essential for the fuel-performance calculations in the sense that the gap evolution was at first incorrectly addressed, with important discrepancies as a result.
- The destructive PIE data of the complementary programme furthermore revealed the non-standard behaviour of the heterogeneous UO_2 fuel, with the development of an important porosity. Inner clad corrosion in some of the fuels indicated elevated oxygen potential, which was not expected on the basis of the fabrication data.
- Regarding modelling efforts, the fact that dynamic data on fission gas release were not available due to the failure of the instrumented pins led us to redefine the scope of the modelling efforts, with an effective reduction on the development of novel fission gas release models. More effort was spent on the analysis of radial distributions (within a fuel pin) of fission and capture.
- The benchmark exercise confirmed that the three fuel-performance codes that participated (TRANSURANUS, COPERNIC and MACROS) are well performing on the established fuels (UO_2 and MOX), but that additional efforts are still needed to achieve a sufficient level of performance for novel fuels such as $(Th,Pu)O_2$. The mechanistic fuel-performance code MACROS achieved predicting the performance of this novel fuel satisfactorily, but further analyses on the effects influencing the results of code calculations will be needed.

5 Tables

5.1 Deliverables list

N°	Short description	Report number	Title	Publication date	Type	Dissemination
D1	Fabrication specifications	EVOL–OMICO–D-01–Rev(4)	Design input data for the fuel segments	01-2002	Re	PU
D2	Irradiation specifications	• EVOL–OMICO–D-02a–Rev(3) • EVOL–OMICO–D-02b–Rev(2)	• Irradiation specifications • Neutronic calculations	• 05-2002 • 07-2002	Re	PU
D3	Properties of $(Th,Pu)O_2$ fuel	EVOL–OMICO–D-03–Rev(1)	Properties of $(Th,Pu)O_2$ fuel	05-2002	Re	PU
D4	Model for the radial power distribution in $(Th,Pu)O_2$ fuel	EVOL–OMICO–D-04–Rev(1)	Model for the radial power distribution in $(Th,Pu)O_2$ fuel	06-2007	Re	PU
D5	Fabrication of fuel pellets and pins and fabrication report	EVOL–OMICO–D-05–Rev(2)	Fuel and Pin fabrication for the OMICO shared cost action.	06-2005	Re	CO, PU
D6	Fuel characterisation report	EVOL-OMICO-D-06	Characterisation report on OMICO fuel pellets – Deliverable 6	04-2007	Re	PU
D7	Design & safety report	EVOL-OMICO-D-07-Rev(1)	Design and Safety report	03-2003	Re	CO
TIP 1	Mid-term T.I.P.		Mid-term TIP	06-2005	Re	PU
D8	Irradiation reports	• EVOL–OMICO–D-08-1–Rev(1) • EVOL-OMICO-D-08-2	• Irradiation report of the OMICO experiment in cycle 2004/5 including a synthesis of the PIE after cycle 2004/5 (cycle 1/10) • Irradiation report of the OMICO experiment (all cycles)	• 05-2005 • 03-2006	Da, Re	RE, PU
D9	Online measurements	EVOL-OMICO-D09	Online measurements cycle 2004/5	03-2006	Da, Re	RE, PU
D10	Non-destructive test reports	• EVOL–OMICO–D-10-T1.1–Rev(1) • EVOL–OMICO–D-10-T1.2–Rev(1) • EVOL–OMICO–D-10-T2.1–Rev(1) • EVOL–OMICO–D-10-T2.2–Rev(1) • EVOL–OMICO–D-10-T3.1	• OMICO PIE on 6 fuel rod segments - Campaign 1 • OMICO PIE campaign 1 Gamma Spectroscopy on 6 fuel segments • OMICO PIE on 6 fuel rod segments - Campaign 2 • OMICO PIE campaign 2 Gamma Spectroscopy on 6 fuel segments • OMICO PIE on 6 fuel rod segments - Campaign 3	• 06-2005 • 06-2005 • 06-2006 • 06-2006 • 03-2007	Da, Re	RE, PU

N°	Short description	Report number	Title	Publication date	Type	Dissemination
		• EVOL–OMICO–D-10-T3.2	• OMICO PIE campaign 3 Gamma Spectrometry on 6 fuel rod segments	• 05-2007		
D11	Benchmarking report	EVOL-OMICO-D-11	Comparison of fuel-performance calculations for the OMICO irradiation experiment	06-2007	Re	PU
~~D12~~	~~Fission gas release model~~		~~Fission gas release model for fuels with a heterogeneous microstructure.~~		~~Th~~	~~PU~~
D12b	Complementary PIE	• EVOL–OMICO–D-12b-T1 • EVOL–OMICO–D-12b-T2 • EVOL–OMICO–D-12b-T3 • EVOL–OMICO–D-12b-T4	• OMICO Complemetary NDT PIE on 6 instrumented fuel rod segments • OMICO Gamma Spectrometry on 6 fuel segments • OMICO Destructive PIE on 3 instrumented fuel rodlets • OMICO Puncture results on two UO_2 segments	06-2007	Re	RE
TIP 2	Final TIP				Re	PU

5.2 Other documents

Report number	Title	Publication year	Dissemination
EVOL-OMICO-R01	OMICO cladding specifications	2002	CO
EVOL-OMICO-R02	Fuel Rod Documentation & Certification relative to the OMICO programme	2002	CO
EVOL-OMICO-R03	Modifications in design and instrumentation of the instrumented fuel rods of OMICO	2002	CO
EVOL-OMICO-R04	TRANSURANUS simulation of the UO2 and MOX fuel rods in the OMICO experiment	2002	CO
EVOL-OMICO-R05	Preliminary simulation of the OMICO experiment with COPERNIC	2002	CO
EVOL-OMICO-R06	Fuel Pellet Specifications for the OMICO and MIMAS-PV Irradiation Experiment	2002	CO
EVOL-OMICO-R07	OMICO and MIMAS-PV Fuel Pin Welding Plan	2003	CO
EVOL-OMICO-R08	OMICO and MIMAS-PV End Cap Welding Qualification No. 1 Non-Instrumented Pins Lower end caps	2003	CO
EVOL-OMICO-R09	OMICO and MIMAS-PV End Cap Welding Qualification No. 2 Non-Instrumented Pins Upper end caps	2003	CO
EVOL-OMICO-R10	OMICO: Non-instrumented pin assembly review	2003	CO
EVOL-OMICO-R11	Corrosion tests on Zircaloy welds: end plugs non-instrumented rods	2003	CO
EVOL-OMICO-R12	OMICO and MIMAS-PV End Cap Welding Qualification No. 3 Instrumented Pins Lower end caps	2003	CO
EVOL-OMICO-R13	Production of Yttria stabilised Hafnia Pellets for the OMICO - MIMAS PV Fuel Pins	2004	CO
EVOL-OMICO-R14	OMICO and MIMAS-PV End Cap Welding Qualification No. 3 Instrumented Pins Lower end caps	2004	CO
EVOL-OMICO-R15	OMICO and MIMAS-PV End Cap Welding Qualification No. 4 Instrumented Pins Upper end caps	2004	CO
EVOL-OMICO-R16	Review of the technical reception of the OMICO and MIMAS-PV fuel rods.	2004	CO
EVOL-OMICO-R17	Corrosion tests on Zircaloy welds: end plugs instrumented rods	2004	CO
EVOL-OMICO-R18	Treatment of pressure and temperature data from the OMICO instrumented fuel rods	2003	CO

6 References

1. Sobolev, V., Wéber, M. & Aoust, T., *Preliminary irradiation conditions*, EVOL-OMICO-D02a-rev3, (Mol, 2002)
2. Sobolev, V. & Van Uffelen, P., *Design input data for the fuel segments*, EVOL-OMICO-D01-rev3, (Mol, 2002)
3. Aoust, T., *Neutronic calculations*, EVOL-OMICO-D02b-rev2, (Mol, 2002)
4. Schubert, A., Lassmann, K. & Van de Laar, J., *TRANSURANUS simulation of the UO2 and MOX fuel rods in the OMICO experiment*, EVOL-OMICO-R04, (Karlsruhe, 2002)
5. Vesco, P., *Preliminary simulation of the OMICO experiment with COPERNIC*, EVOL-OMICO-R05, (Lyon, 2002)
6. Toury, G., Holzhäuser, M., Boshoven, C., Selfslag, C., Naisse, F., Zentz, A., Hein, H., Voet, R., Modery, M., Murray, M., McGinley, J. & Somers, J., *Fuel and Pin fabrication for the OMICO shared cost action.*, EVOL-OMICO-D05-rev2, (Karlsruhe, 2005)
7. Toury, G., Holzhäuser, M., Boshoven, C., Naisse, F., Accarier, A., Hein, H., Voet, R., Modery, M., Murray, M., Staicu, D. & Somers, J., *Characterisation report on OMICO fuel pellets - Deliverable D6*, EVOL-OMICO-D06, (Karlsruhe, 2005)
8. Fink, J. K. (2000) *Journal of Nuclear Materials* **279,** 1-18.
9. Duriez, C., Alessandri, J. P., Gervais, T. & Philipponeau, Y. (2000) *J. Nucl. Mater.* **277,** 143.
10. Pillai, C. G. S. & et.al. (2000) *J. Nucl. Mater.* **277,** 116
11. Inoue, N. (2000) *J. Nucl. Mater.* **282,** 186
12. Wéber, M., *The Experimental Rig - Detailed Design and Safety Report*, EVOL-OMICO-D07, (Mol, 2003)
13. Verwerft, M., Vermeeren, L., Gouat, P., Wéber, M., Kuzminov, V. & Borms, L., *Irradiation report of the OMICO experiment in cycle 2004/5 including a synthesis of the PIE after cycle 2004/5 (cycle 1/10).* EVOL-OMICO-D08.1, (Mol, 2005)
14. Verwerft, M., Borms, L., Parthoens, Y., Willekens, M., Vermeeren, L., Gouat, P., Kuzminov, V. & Wéber, M., *Irradiation report of the OMICO experiment (all cycles)*, EVOL-OMICO-D08b, (Mol, 2007)
15. Wéber, M., Coupé, B., Gouat, P., Vermeeren, L. & Verwerft, M., *Overview of the OMICO Irradiation Campaigns in CALLISTO*, EVOL-OMICO-D09, (Mol, 2007)
16. Vermeeren, L., Dekeyser, J., Gouat, P., Kalcheva, S., Koonen, E., Kuzminov, V., Verwimp, A. & Wéber, M., *Qualification of the online power determination of fuel elements in irradiation devices in the BR2 reactor.*, SCK•CEN-BLG-1006, (Mol, 2005)
17. Borms, L., Gys, A. & Parthoens, Y., *OMICO, PIE campaign 1 - Gamma Spectroscopy on 6 fuel segments*, EVOL-OMICO-D10-T1.2, (Mol, 2005)
18. Parthoens, Y., Gys, A. & Van den Berghe, S., *OMICO, PIE campaign 2 - Gamma Spectroscopy on 6 fuel segments*, EVOL-OMICO-D10-T2.2, (Mol, 2006)
19. Parthoens, Y., Jutier, F., Gys, A., Borms, L. & Van den Berghe, S., *OMICO, PIE campaign 3 - Gamma Spectroscopy on 6 fuel segments*, EVOL-OMICO-D10-T3.2, (Mol, 2007)
20. Parthoens, Y., Gys, A. & Sannen, L., *OMICO PIE on 6 fuel rod segments – Campaign 1*, EVOL-OMICO-D10-T1.1, (Mol, 2005)

21. Parthoens, Y., Gys, A. & Van den Berghe, S., *OMICO PIE on 6 fuel rod segments - Campaign 2*, EVOL-OMICO-D10-T2.1, (Mol, 2006)
22. Parthoens, Y., Gys, A. & Van den Berghe, S., *OMICO PIE on 6 fuel rod segments - Campaign 3*, EVOL-OMICO-D10-T3.1, (Mol, 2007)
23. Parthoens, Y., Gys, A. & Van den Berghe, S., *OMICO Complementary NDT on 6 fuel rod segments*, EVOL-OMICO-D12b-T1, (Mol, 2007)
24. Jutier, F., Parthoens, Y., Gys, A., Borms, L. & Van den Berghe, S., *OMICO, Gamma Spectroscopy on 6 instrumented fuel segments*, EVOL-OMICO-D12b-T2, (Mol, 2007)
25. Vos, B. & Van den Berghe, S., *OMICO, Destructive PIE on three fuel rodlets*, EVOL-OMICO-D12b-T3, (Mol, 2007)
26. Vos, L., Gys, A. & Adriaensen, L., *OMICO Fission gas puncture and mass spectrometric analysis - rods A and C*, EVOL-OMICO-D12b-T4, (Mol, 2007)
27. Lemehov, S. E. & Govers, K., *Model for the radial power distribution in (Th,Pu)O2 fuel*, EVOL-OMICO-D04, (Mol, 2007)
28. Schubert, A., Segura, H., Verwerft, M. & Lemehov, S. E., *Comparison of fuel-performance calculations for the OMICO irradiation experiment*, EOL-OMICO-D11, (Karlsruhe, 2007)